

Molecular Hydrogen in the Damped Ly α Absorber of Q1331+170

Jun Cui¹, Jill Bechtold¹, Jian Ge², and David M. Meyer³

ABSTRACT

We used HST/STIS to obtain the spectrum of molecular hydrogen associated with the damped Ly α system at $z_{\text{abs}} = 1.7765$ toward the quasar Q1331+170 at $z_{\text{em}} = 2.084$. Strong H₂ absorption was detected, with a total H₂ column density of $N(\text{H}_2) = (4.45 \pm 0.36) \times 10^{19} \text{ cm}^{-2}$. The molecular hydrogen fraction is $f_{\text{H}_2} = \frac{2N_{\text{H}_2}}{N_{\text{HI}} + 2N_{\text{H}_2}} = (5.6 \pm 0.7)\%$, which is the greatest value reported so far in any redshifted damped Ly α system. This results from the combined effect of a relatively high dust-to-gas ratio, a low gas temperature, and an extremely low ambient UV radiation field. Based on the observed population of J states, we estimate the photo-absorption rate to be $R_{\text{abs}} = (7.6 \pm 2.4) \times 10^{-13} \text{ s}^{-1}$, corresponding to a local UV radiation field of $J(1000\text{\AA}) \approx 2.1 \times 10^{-3} J_{1000\text{\AA},\odot}$, where $J_{1000\text{\AA},\odot}$ is the UV intensity at 1000 \AA in the solar neighborhood. This is comparable with the metagalactic UV background intensity at this redshift, and implies an extremely low star formation rate in the absorber's environment. We construct a simple model to describe the structure of the H₂ absorber, with a best-fit total hydrogen number density of $n(\text{H}) \approx 0.2 \text{ cm}^{-3}$ and an electron temperature of $T_e \approx 140 \text{ K}$. Assuming spherical symmetry, the mass of the H₂ cloud is estimated to be $\approx 6.5 \times 10^7 M_\odot$, larger than the masses of most giant molecular clouds (GMCs) in the Milky Way and nearby galaxies. The extinction of Q1331+170 due to the intervening DLA is $E_{\text{B}-\text{V}} \approx 0.037$, and we also find that the extinction by DLAs with firm H₂ detections is significantly greater than those for which only upper limits of f_{H_2} have been put. The observed CO-to-H₂ column density ratio is $\frac{N_{\text{CO}}}{N_{\text{H}_2}} < 2.5 \times 10^{-7}$, which is similar to the value measured for diffuse molecular clouds in the Galactic ISM. Finally, applying the inferred physical conditions to the observed C I fine structure excitation (Songaila *et*

¹Steward Observatory, University of Arizona, 933 N Cherry Avenue, Tucson, AZ 85721, USA; Email: jcui@as.arizona.edu

²Dept. of Astronomy, University of Florida, 210 Bryant Space Science Center, Gainesville, FL 32611, USA

³Dept. of Physics and Astronomy, Northwestern University, 2145 Sheridan Road, Evanston, IL 60208, USA

al. 1994), we estimate the cosmic microwave background temperature to be $T_{\text{CMB}} = (7.2 \pm 0.8)$ K at $z = 1.77654$, consistent with the predicted value of 7.566 K from the standard cosmology.

Subject headings: quasars: absorption lines — quasars: individual (Q1331+170) — ISM: molecules

1. Introduction

Damped Ly α absorbers (hereafter DLAs) are defined as quasar absorption systems with neutral hydrogen column density, $N(\text{HI}) > 2 \times 10^{20} \text{ cm}^{-2}$. They are generally considered to be progenitors of present-day galaxies, in the form of fast rotating disks (Prochaska & Wolfe 1997), or merging protogalactic clumps (Haehnelt *et al.* 1998). They serve as an important gas reservoir for star formation at high redshifts (e.g. Storrie-Lombardi & Wolfe 2000).

Molecular gas, especially molecular hydrogen, is an important ingredient of star formation, since stars form by cooling via molecular lines. The search for H₂ in DLAs can be carried out by observing the H₂ absorption lines in the Lyman $\text{X}^1\Sigma_g^+ \rightarrow \text{B}^1\Sigma_u^+$ and Werner $\text{X}^1\Sigma_g^+ \rightarrow \text{C}^1\Sigma_u^\pm$ bands, with rest wavelengths from $\sim 1220\text{\AA}$ to the Lyman limit (Abgrall *et al.* 1993a, 1993b). Ge & Bechtold (1999) conducted a survey for H₂ absorption in 13 DLAs, using the MMT Spectrograph. Two have been confirmed with significant H₂ fraction; upper limits in the range of 10^{-6} to 10^{-4} were put on the H₂ fraction in other systems (Ge & Bechtold 1997, 1999, Ge *et al.* 2001). More recently, based on the high resolution spectra obtained with UVES at the ESO VLT, Ledoux *et al.* (2003) searched for H₂ in a sample of 33 DLAs, with firm detections of H₂ absorption in 8 of them. By contrast, almost every line of sight through Galactic or Magellanic gas clouds with comparable H I column density has strong H₂ absorption (e.g. Shull *et al.* 2000).

In the interstellar medium, H₂ molecules are expected to form on the surface of dust grains by physical or chemical adsorption (Cazaux & Tielens 2002). Therefore one contributing factor to the lack of H₂ in DLAs is the low dust-to-gas ratios in these systems (e.g. Pei *et al.* 1991, Pettini *et al.* 1994, Vladilo 1998, Prochaska & Wolfe 2002), perhaps the result of the fact that quasar surveys tend to select objects which are bright and blue (e.g. Gregg *et al.* 2002, Khare *et al.* 2004). A second contributing factor to the lack of H₂ may be the high gas temperature in DLAs which makes H₂ formation onto dust grains inefficient (Petitjean *et al.* 2000, Liszt 2002). This is consistent with the suggestion that unlike the local ISM, the gas in DLAs might be predominantly warm (Lu *et al.* 1996, Prochaska & Wolfe 1999). Finally, H₂ molecules are easily dissociated by UV photons in the energy range of 11.3 —

13.6 eV. Therefore the low H_2 fraction in DLAs may be the result of a strong UV radiation field (e.g. Black *et al.* 1987), which could in turn be a signature of high star formation rate (Wolfe *et al.* 2003a, 2003b, 2004). Recently, Hirashita *et al.* (2003) showed that the deficiency of H_2 in DLAs may also be a result of the expected low volume filling factor of H_2 in environments with a strong UV radiation field and low dust-to-gas ratio, rather than a real absence of H_2 .

Q1331+170 (at $z_{\text{em}} = 2.084$) is one of the first high redshift quasars discovered (Baldwin *et al.* 1973), and has a damped Ly α absorber at $z = 1.7765$ (Carswell *et al.* 1975) with a neutral hydrogen column density of $N_{\text{HI}} = 1.5 \times 10^{21} \text{ cm}^{-2}$ (Chaffee *et al.* 1988, Prochaska & Wolfe 1999). The 21-cm absorption line was also detected (Wolfe & Davis 1979, Chengalur & Kanekar 2000), with a spin temperature of $T_s \approx 770 \text{ K}$. This implies the presence of a cold neutral medium (CNM) phase conducive to the efficient formation of H_2 onto dust grains (Petitjean *et al.* 2000). One of the most interesting features in the absorption spectrum of Q1331+170 is the presence of strong C I and C I* multiple lines near $\lambda \sim 1656 \text{ \AA}$ (Meyer *et al.* 1986, Songaila *et al.* 1994). C I absorption has been found to be rare in quasar absorbers as compared to Galactic diffuse clouds as a result of higher UV radiation fields, or lower dust abundances (Ge *et al.* 1997, 2001). Since these conditions would also be inhospitable to an appreciable formation of H_2 , the damped Ly α absorber toward Q1331+170 is an excellent candidate for a search for H_2 absorption.

Detecting C I is also of cosmological interest, since it is insensitive to the local physical conditions, but depends strongly on the cosmic background level (Liszt 2002). Therefore the fine structure transitions of C I can be used to measure the CMB temperature as a function of redshift (e.g. Bahcall *et al.* 1973). In the case of the DLA toward Q1331+170, the excitation temperature of neutral carbon determined by Songaila *et al.* (1994) is $7.4 \pm 0.8 \text{ K}$ for one of two velocity components at $z = 1.77654$, in agreement with the predicted value of $T_{\text{CMB}} = 7.566 \text{ K}$ at that redshift. This result implies that local excitation of C I is negligible. Since the population of H_2 at different J states can also be used to determine physical parameters, such as kinetic temperature, neutral hydrogen number density, and UV radiation field, observations of molecular hydrogen and its rotational excitation provide an independent verification of the observed C I excitation.

In this paper, we present our detection of redshifted H_2 in the high resolution absorption spectrum of Q1331+170 taken with the *Space Telescope Imaging Spectrograph* (STIS) aboard the *Hubble Space Telescope* (HST). Sec. 2 describes the observations and basic data reductions. In Sec. 3, we describe the Voigt profile fitting of H_2 lines, and present the best-fit physical parameters. Discussions are presented in Sec. 4, and conclusions in Sec. 5.

2. Observations and continuum fitting

In HST GO programs 7271 and 9172, we used HST/STIS to obtain the near UV spectrum of Q1331+170 in the wavelength range of 2500Å to 3120Å. The spectrum was obtained with the E230M grating with $0.2'' \times 0.2''$ aperture, and the NUV/MAMA detector in the ACCUM operating mode, resulting in spectral resolution of $R = 30,000$ (or 10 km s^{-1}) at $\lambda \sim 2700\text{\AA}$. The total exposure time was 52,298 seconds, yielding spectra with $\text{S/N} \sim 7$ above the Lyman limit of the damped Ly α absorber ($\sim 2530\text{\AA}$). The data sets are listed in Table 1.

The data were pre-processed with the IRAF calibration routine CALSTIS (v2.7) for nonlinearity correction, dark subtraction, flat-fielding, wavelength calibration, and extraction of the 1-D spectrum. Rebinning was performed on the raw images for Nyquist sampling (i.e. 2 pixels per resolution element). Instead of using automatic wavelength calibration files taken for each Mode Selection Mechanism (MSM) setting, we obtained additional exposures of comparison lamps during each orbit. Typical observing conditions may cause thermal drifts of 0.1 pixel per hour (see Sec. 11.2 of *Space Telescope Imaging Spectrograph Instrument Handbook for Cycle 13* for more details). For our longest single exposure, this corresponds to a wavelength uncertainty of $\sim 0.007\text{\AA}$ at $\lambda \sim 2700\text{\AA}$ introduced by wavelength calibration, or a velocity uncertainty of $\sim 0.8 \text{ km s}^{-1}$.

The entire flux-calibrated spectrum of Q1331+170 is shown in Fig. 1, smoothed by 5 pixels. The continuum was determined by a 4th order polynomial fit using the data longward of the Lyman limit of the DLA ($\approx 2530\text{\AA}$). Regions with strong absorption features identified by eye were excluded. The dotted line in Fig. 1 shows the 1σ uncertainties of the observed spectrum. The continuum fit suffers from considerable uncertainties, due to the numerous absorption features in the Ly α forest, as well as H₂ absorption lines in the Lyman and Werner bands. For this reason, we checked our continuum fit according to the following prescription. We separate the whole spectrum into several continuous wavelength regions, and for each region, we construct the histogram of all the data points with normalized flux greater than 1. Ideally, the histogram can be well represented by a (half-)Gaussian distribution with a standard deviation corresponding to the normalized 1σ error of our spectrum. Next, we adjust the best-fit continuum in the region under consideration until the calculated Gaussian standard deviation is approximately equal to the average normalized 1σ error in the same region. The above procedure was performed in an iterative manner, since an adjustment of the continuum also changes the (normalized) 1σ error used for comparison. This procedure can be used to determine both the overall amplitude and shape of the continuum.

We estimate the accuracy of continuum fitting by calculating the reduced χ^2 -deviation between the probability distribution function (PDF) of normalized flux adopting the best-fit

Table 1. Log of HST/STIS observations

Dataset	Program	UT date of observation	Exposure (sec)
o56m0101	7271	1999-08-20	2076
o56m0102	7271	1999-08-20	5794
o56m0201	7271	1999-08-21	2076
o56m0202	7271	1999-08-21	5794
o6cy0101	9172	2002-07-08	2097
o6cy0102	9172	2002-07-08	5794
o6cy0201	9172	2002-08-12	2097
o6cy0202	9172	2002-08-12	5794
o6cy0301	9172	2002-08-19	2097
o6cy0302	9172	2002-08-19	5794
o6cy0401	9172	2002-08-19	2097
o6cy0402	9172	2002-08-19	5794
o6cy0501	9172	2003-03-16	2097
o6cy0502	9172	2003-03-16	5794
o6cy0601	9172	2003-03-12	2097
o6cy0602	9172	2003-03-12	5794
o6cy0701	9172	2002-07-10	2097
o6cy0702	9172	2002-07-10	2897

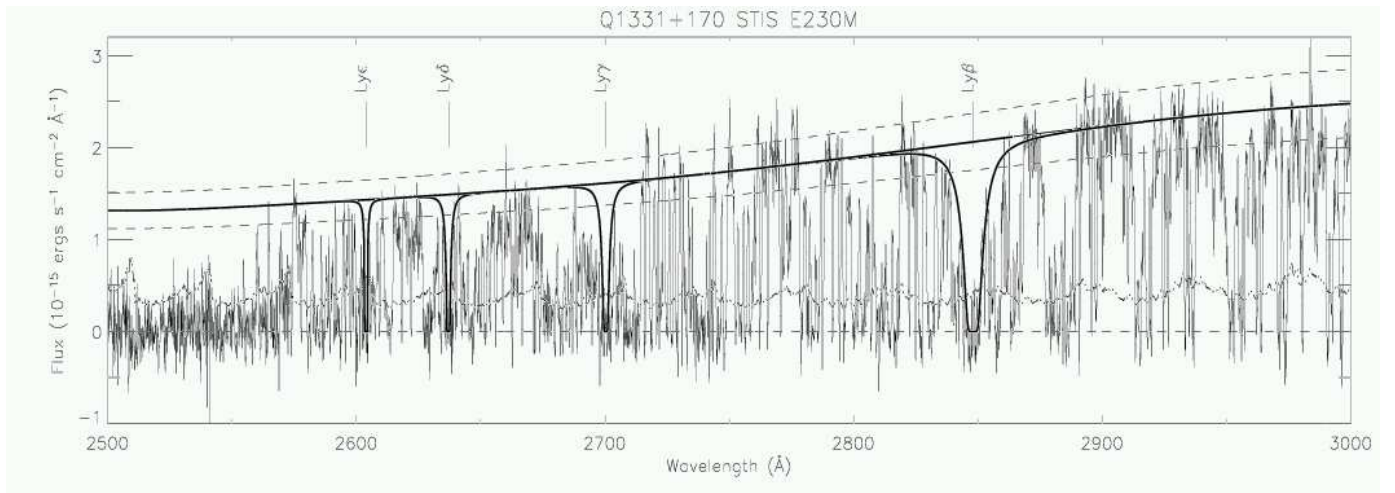


Fig. 1.— The STIS E230M spectrum of Q1331+170. The best-fit continuum (the thick solid line) is superposed on the flux-calibrated spectrum. The dotted line corresponds to 1σ uncertainties of the observed spectrum. The data have been smoothed by 5 pixels. The two dashed lines represent the best-fit continuum scaled 15% lower and 15% higher. Also shown on the figure are the synthetic profiles of Lyman series lines, including Ly β , Ly γ , Ly δ and Ly ϵ . The synthetic profiles are calculated with a neutral hydrogen column density of 1.5×10^{21} cm⁻² and a b -parameter of 19.6 km s⁻¹ (see text).

continuum and that with continuum level scaled by a certain factor (ranging from 50% lower to 50% higher). Here only pixels with normalized flux greater than 1 are considered. This calculation shows that the best-fit continuum is accurate within 15% at 83% confidence level, and accurate within 25% at 98% confidence level, based on the χ^2 distribution.

The two dashed lines in Fig. 1 correspond to the best-fit continuum scaled 15% lower and 15% higher. This represents a very conservative estimate of the uncertainty in the continuum fit; clearly the dashed lines are inconsistent with the expected continuum level in portions of the spectrum. The effects of the possible uncertainties in continuum fitting on our final results are discussed in Sec. 3.3.

3. Analysis of molecular hydrogen lines

3.1. Detection of molecular hydrogen

Previous spectroscopic studies show that there are at least five redshift systems with detectable metal absorption lines along the line of sight toward Q1331+170. They include the damped Ly α system at $z = 1.7765$, as well as absorbers at $z = 0.7441$ (Sargent *et al.* 1988), $z = 1.3284$ (Steidel & Sargent 1992), $z = 1.4458$ (Sargent *et al.* 1988) and $z = 1.7864$ (Lanzetta *et al.* 1987).

We searched for molecular hydrogen absorption associated with the $z = 1.7765$ DLA and two other absorbers at $z = 1.4458$ and $z = 1.7864$, since their redshifts allow considerable overlap between the wavelength coverage of our spectrum and the redshifted Lyman and Werner bands of H₂. By comparing with the synthetic H₂ spectrum, we detected strong molecular hydrogen absorption associated with the $z = 1.7765$ damped Ly α system, whereas the H₂ line pattern does not match the observed spectrum for the other two absorbers.

For the damped Ly α system at $z = 1.7765$, we calculated the significance level of H₂ lines for each J state. We define the significance level, SL associated with state J as

$$SL = \frac{\sum_i \int [1 - f_i(\lambda)] d\lambda}{[\sum_i \int \sigma_i^2(\lambda) d\lambda]^{1/2}}, \quad (1)$$

where $f_i(\lambda)$ and $\sigma_i(\lambda)$ are the normalized flux and 1σ error within an individual H₂ line, and the summation is over all the selected H₂ lines for the same J state. The results show that based on our spectrum, $J = 0, 1, 2, 3, 4$ lines are detectable at 4.4σ , 5.1σ , 9.0σ , 8.9σ and 3.7σ significance level, respectively. The $J \geq 5$ lines were not detected at 3σ significance level. The number of unblended H₂ lines included in the above calculation is two for $J = 0$, three for $J = 1$, six for $J = 2$, ten for $J = 3$, two for $J = 4$, and five for $J = 5$, respectively

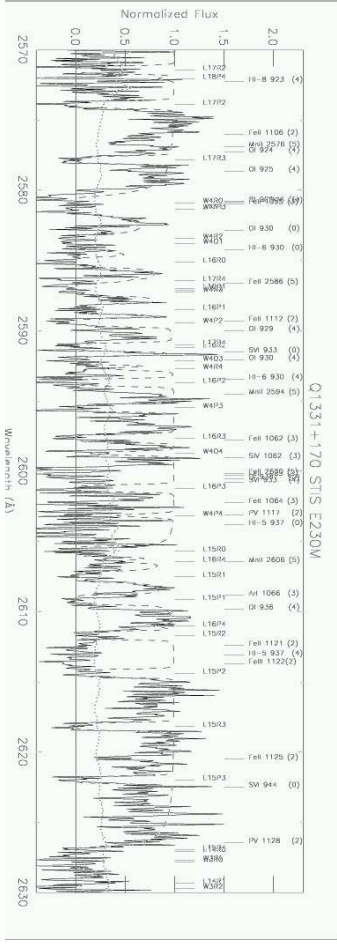
(see also Table 2). Therefore, we conclude that we detect molecular hydrogen absorption from the $J = 0$ to $J = 4$ states, associated with the damped Ly α system at $z = 1.7765$.

In Fig. 2, we mark the expected positions of metal lines from all the known absorbers, including the Milky Way interstellar medium, on the observed spectrum (solid line) with 1σ errors (dotted line). The atomic line list was taken from Table 2 of Prochaska *et al.* (2001). Also marked on Fig. 2 are all the H_2 lines from $J = 0$ to 4 in the Lyman and Werner bands for the $z = 1.7765$ absorber.

3.2. Voigt profile fitting of molecular hydrogen lines

We used VPFIT (version 5) to simultaneously fit Voigt profiles for all the H_2 lines. All lines with $J = 0, 1, 2, 3$ and 4 were fit simultaneously, assuming one b -parameter and redshift for all lines and different column densities for each J state. These free parameters were adjusted independently to minimize the χ^2 value of the overall fitting. We adopted the STIS instrument profile for the echelle E230M and $0.2'' \times 0.2''$ aperture. Those H_2 lines with large reduced χ^2 deviations ($\chi^2_\nu > 1.2$) were excluded, to avoid possible cases in which H_2 absorption may be contaminated by Ly α forest lines. This procedure was iterated until no more lines were rejected. Our final model includes 20 different regions with 26 molecular hydrogen lines for simultaneous fitting (two $J = 0$ lines, three $J = 1$ lines, seven $J = 2$ lines, twelve $J = 3$ lines and two $J = 4$ lines). We also note that the physical parameters determined from Voigt profile fitting (see below) are insensitive to our adopted maximum reduced χ^2 deviation of 1.2.

Table 2 provides the results for all the H_2 lines included in the final fitting. Rest-frame wavelengths, f -values and damping parameters Γ are taken from Abgrall *et al.* (1993a, 1993b). The sixth column gives the reduced χ^2 value for all the 20 fitted regions. We show the best-fit Voigt profiles for different H_2 lines in Fig. 3 (solid lines), superposed on the observed spectrum with 1σ errors. The Voigt profiles for all the H_2 lines with $J = 0$ to 4 in the Lyman and Werner bands are also shown by the dashed line in Fig. 2.



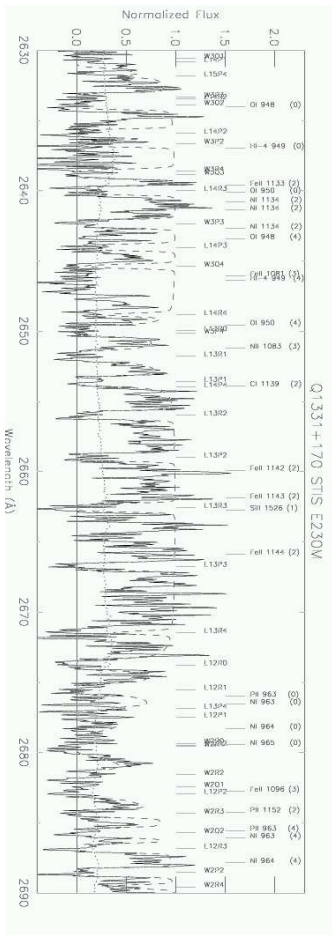


Fig. 2b.— Same as Fig. 2a.

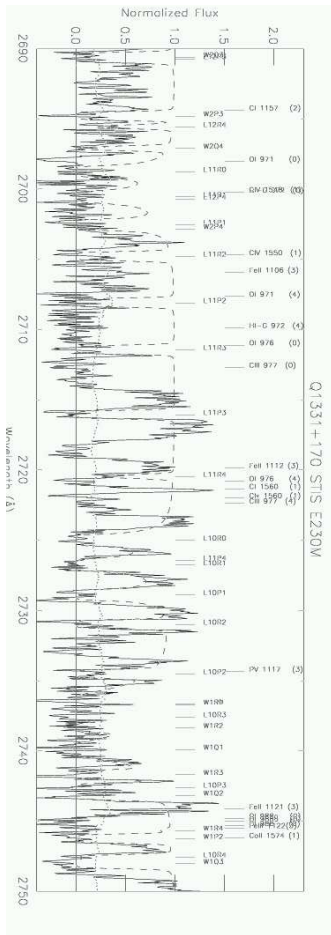


Fig. 2c.— Same as Fig. 2a.

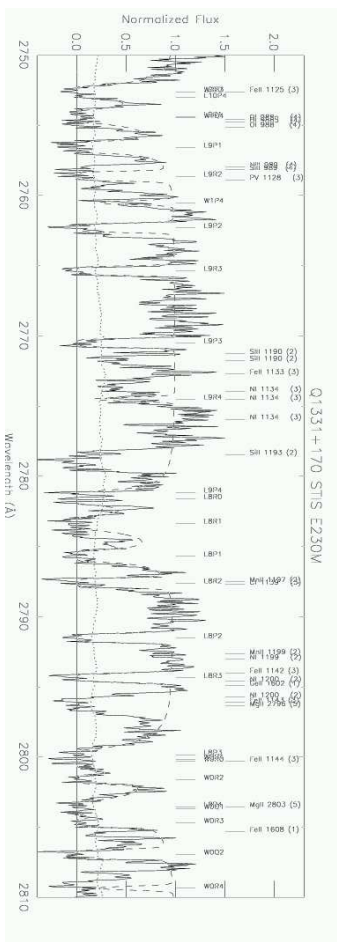


Fig. 2d.— Same as Fig. 2a.

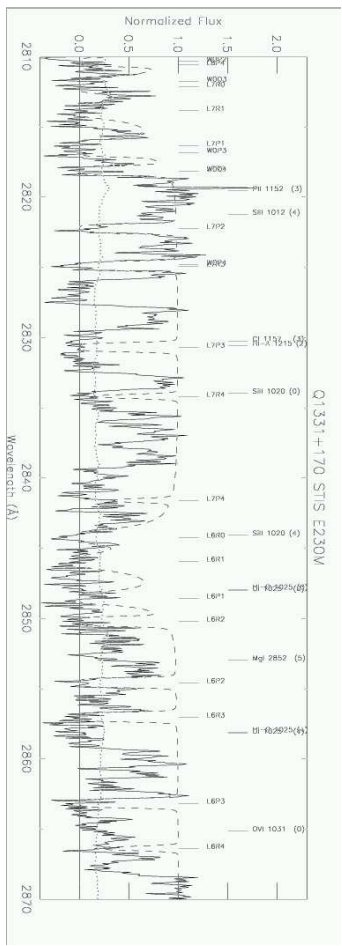


Fig. 2e.— Same as Fig. 2a.

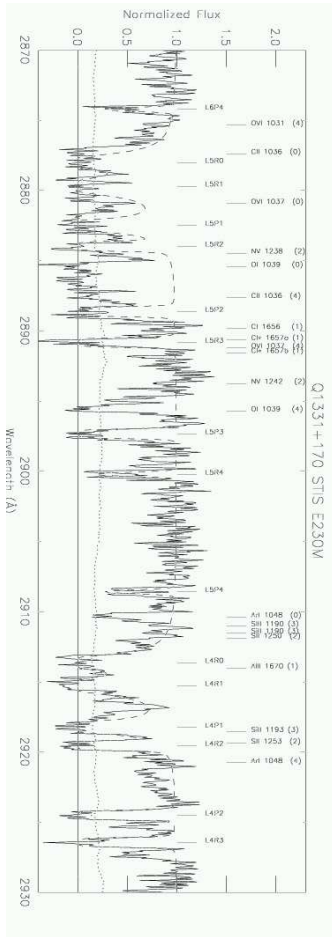


Fig. 2f.—Same as Fig. 2a.

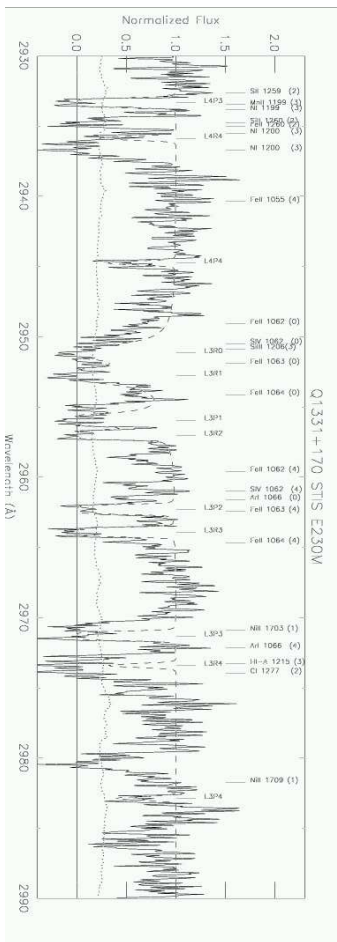


Fig. 2g.—Same as Fig. 2a.

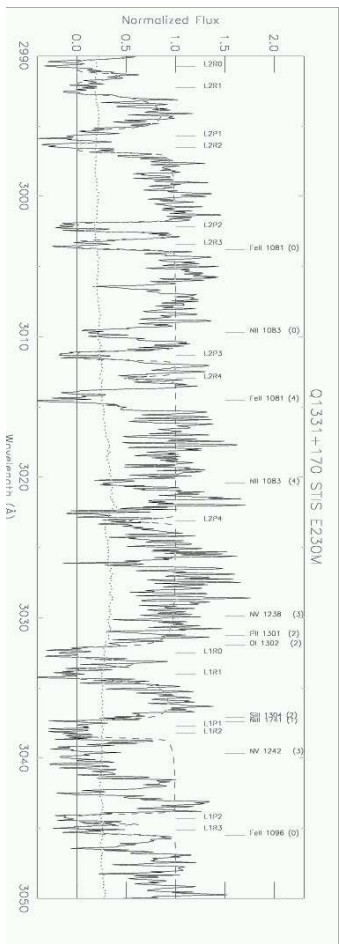


Fig. 2h.— Same as Fig. 2a.

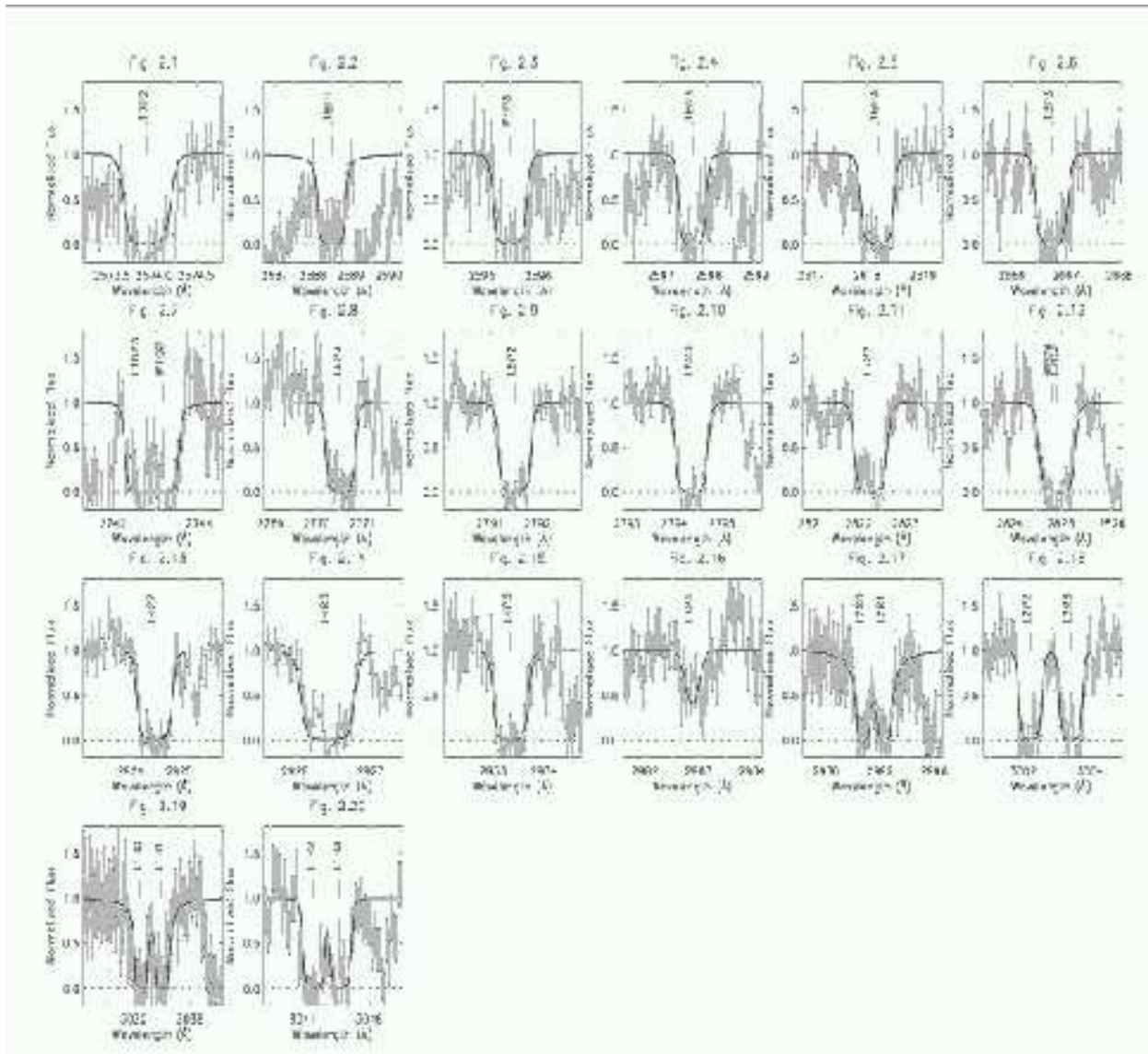


Fig. 3.— The best-fit Voigt profiles for the 26 H₂ lines used in our simultaneous fitting (solid lines), overplotted on the observed profiles with 1 σ errors.

Table 2. H_2 absorption lines associated with the DLA toward Q1331+170

No.	Identification	λ_{rest} (Å)	f (10^{-2})	Γ (10^9 s^{-1})	χ^2_ν
1	L17P2	927.02	0.233	0.804	1.01
2	L16P1	932.27	0.240	0.835	0.32
3	W4P3	934.79	0.709	1.101	0.90
4	L16R3	935.57	0.657	0.830	0.80
5	L15R3	942.96	0.574	0.862	1.06
6	L13P3	960.45	0.493	0.939	0.73
7	L10P3	987.77	0.893	1.070	1.10
	W1Q2	987.97	3.650	1.157	
8	L9P3	997.82	0.876	1.120	0.76
9	L8P2	1005.39	0.991	1.177	0.46
10	L8R3	1006.41	1.572	1.167	0.73
11	L7P2	1016.46	1.023	1.236	0.72
12	W0P4	1017.38	0.995	1.178	1.10
	L7R3	1017.42	1.838	1.224	
13	L4P2	1053.28	0.902	1.448	0.70
14	L4R3	1053.98	1.336	1.434	0.85
15	L4P3	1056.47	0.956	1.445	0.59
16	L3P4	1074.31	0.774	1.525	0.98
17	L2R0	1077.14	1.166	1.630	0.62
	L2R1	1077.70	0.769	1.626	
18	L2P2	1081.27	0.470	1.630	0.93
	L2R3	1081.71	0.636	1.613	
19	L1R0	1092.19	0.578	1.738	0.88
	L1R1	1092.73	0.378	1.734	
20	L1P2	1096.44	0.237	1.738	0.94
	L1R3	1096.73	0.305	1.719	

The best-fit results of H_2 column densities, b -parameter and redshift are listed in Table 3. The 1σ errors were derived from χ^2 fitting by VPFIT, and are mainly dependent on photon statistics. The total molecular hydrogen column density is $N_{\text{H}_2} = (4.45 \pm 0.36) \times 10^{19} \text{ cm}^{-2}$. We can place an upper limit on the $J = 5$ column density as $N_{J=5} \leq 6.3 \times 10^{13} \text{ cm}^{-2}$, at 2σ significance level. The 1σ error in redshift given in Table 3 corresponds to the uncertainty in line centroiding, which is equivalent with 0.9 km s^{-1} in velocity space. We mentioned in Sec. 2 that the velocity uncertainty caused by wavelength calibration is 0.8 km s^{-1} . Therefore the total 1σ error is 1.2 km s^{-1} , which is about 10% of the spectral resolution.

The molecular hydrogen fraction is defined as

$$f_{\text{H}_2} = \frac{2N_{\text{H}_2}}{N_{\text{HI}} + 2N_{\text{H}_2}}. \quad (2)$$

Adopting a neutral hydrogen column density of $N_{\text{HI}} = (1.50 \pm 0.14) \times 10^{21} \text{ cm}^{-2}$ (Prochaska & Wolfe 1999), we derived a molecular hydrogen fraction of $f_{\text{H}_2} = (5.6 \pm 0.7)\%$. This is the largest value reported so far in any redshifted damped Ly α system. The profiles of the Lyman series lines are shown in Fig. 1, assuming $N_{\text{HI}} = 1.50 \times 10^{21} \text{ cm}^{-2}$ and $b = 19.6 \text{ km s}^{-1}$. The b -parameter is directly scaled from the b -parameter determined from Voigt profile fitting of molecular hydrogen lines, taking into account the difference in particle mass between the two species. The synthetic line profiles are in broad agreement with the observations. The fact that H I lines are heavily blended with other H_2 lines makes Voigt profile fitting to derive N_{HI} difficult. Therefore we simply adopt the neutral hydrogen column density from previous work (Prochaska & Wolfe 1999).

3.3. Uncertainties due to curve-of-growth and continuum fitting

The uncertainties in the measured H_2 column densities at different J states depend on the location of the corresponding lines on the curve of growth. We show in Fig. 4 the curve of growth for the 26 H_2 lines used in our simultaneous Voigt profile fitting. Note that the equivalent widths are calculated with the best-fit parameters shown in Table 3, since some of the lines are blended and therefore not appropriate for direct measurements of equivalent widths from the observed spectrum. Lines with different J values are marked with different symbols. The background dots in Fig. 4 bracket the full range of the curve of growth for H_2 lines, taking into account the variations in the atomic data (Abgrall *et al.* 1993a, 1993b). The figure shows that the $J = 0, 1$ lines lie on the damped part of the curve of growth, while $J = 2, 3$ lines on the flat part, and $J = 4$ lines on the linear part of the curve of growth. Since the determination of column densities is very sensitive to the choice of b -parameter on the flat part of the curve of growth, the uncertainties in $N_{J=2}$ and $N_{J=3}$ are relatively

larger than the column densities at lower J states. Although $J = 4$ lines are on the linear part of the curve of growth, the 1σ error in $N_{J=4}$ is also relatively large due to the low signal-to-noise ratio for these weaker lines.

Uncertainties in column density are also likely introduced by uncertainties in continuum fitting. To investigate this effect, we scaled our continuum by a factor ranging from 25% lower to 25% higher than the best-fit continuum. Then we did simultaneous Voigt profile fitting in the same way as described in Sec. 3.2. The results are shown in Fig. 5, for the measured column densities at different J states. We find that the errors in column density at all J states caused by 1σ uncertainties in continuum fit are considerably smaller than the 1σ error in column density derived from Voigt profile fitting. In the extreme case that if our best-fit continuum is under-estimated by a factor of 25% (which can be excluded by 98% confidence level, see Sec. 3.2), the corresponding uncertainties in H_2 column densities at $J = 2$ and 3 can be relatively large. Fortunately, the physical state in the H_2 absorber is not sensitive to $N_{J=2,3}$ (see Sec. 4.1 for more details). Therefore we conclude that our final results are not critically dependent on the uncertainties in continuum fitting.

3.4. Excitation temperature

Once the H_2 column densities at different J states are determined, we can calculate the excitation temperature for each $J \geq 1$ state by the Boltzmann law

$$\frac{N_J}{N_0} = \frac{g_J}{g_0} \exp \left[-\frac{\epsilon_J - \epsilon_0}{kT_{\text{ex}}} \right], \quad (3)$$

where $\epsilon_J - \epsilon_0$ is the excitation energy of level J relative to the ground state, k is the Boltzmann constant, the degeneracy is $g_J = (2I+1) \times (2J+1)$, and I is the nuclear spin (0 for even J and 1 for odd J). Fig. 6 shows the plot of $\log \frac{N_J}{g_J}$ for each J state as a function of its excitation potential, with 1σ errors. The populations of the five detected J states can be well fitted by a single temperature Boltzmann distribution, with $\chi^2_{\nu} = 0.20$. The one-temperature model is shown by the solid line in Fig. 6, with a best-fit excitation temperature of $T_{\text{ex}} = (152 \pm 10)$ K. The upper limit put on $N_{J=5}$ is also consistent with this model. Increasing or decreasing the best-fit continuum by 15% results in a similar excitation model with the best-fit excitation temperature of $T_{\text{ex}} = (153 \pm 10)$ K or $T_{\text{ex}} = (150 \pm 10)$ K, respectively. The insensitivity of T_{ex} to the continuum fitting partly results from the logarithmic dependence of T_{ex} on the ratio of column densities.

A unique temperature for rotational excitation of H_2 is not characteristic of Galactic H_2 clouds, and the populations of rotational states of H_2 often require at least two different excitation temperatures (e.g. Spitzer & Cochran 1973). T_{ex} for the low J states approximates

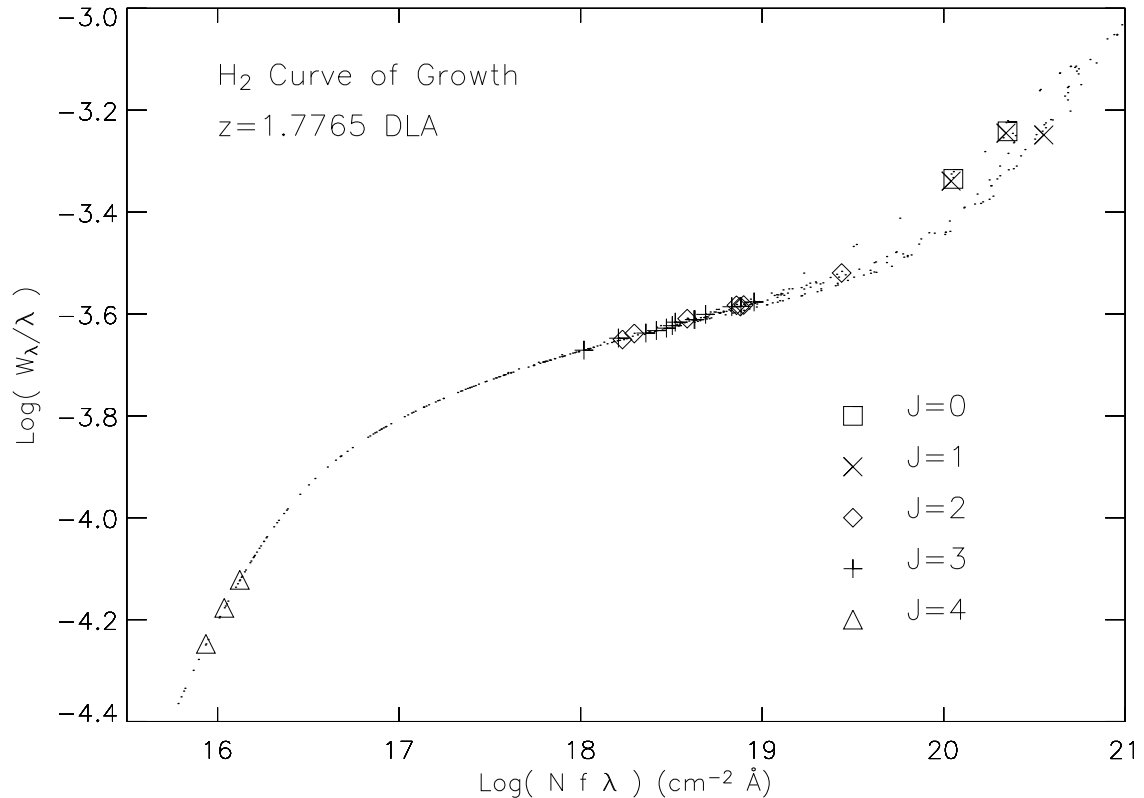


Fig. 4.— The curve of growth for H₂ lines identified in the spectrum of Q1331+170. Different symbols stand for transitions from different J states. The background dots bracket the full range of the curve of growth for H₂ lines, taking into account variations in the atomic data. The $J = 0, 1$ lines are on the damped part of the curve of growth, the $J = 2, 3$ lines on the flat part, and the $J = 4$ lines on the linear part.

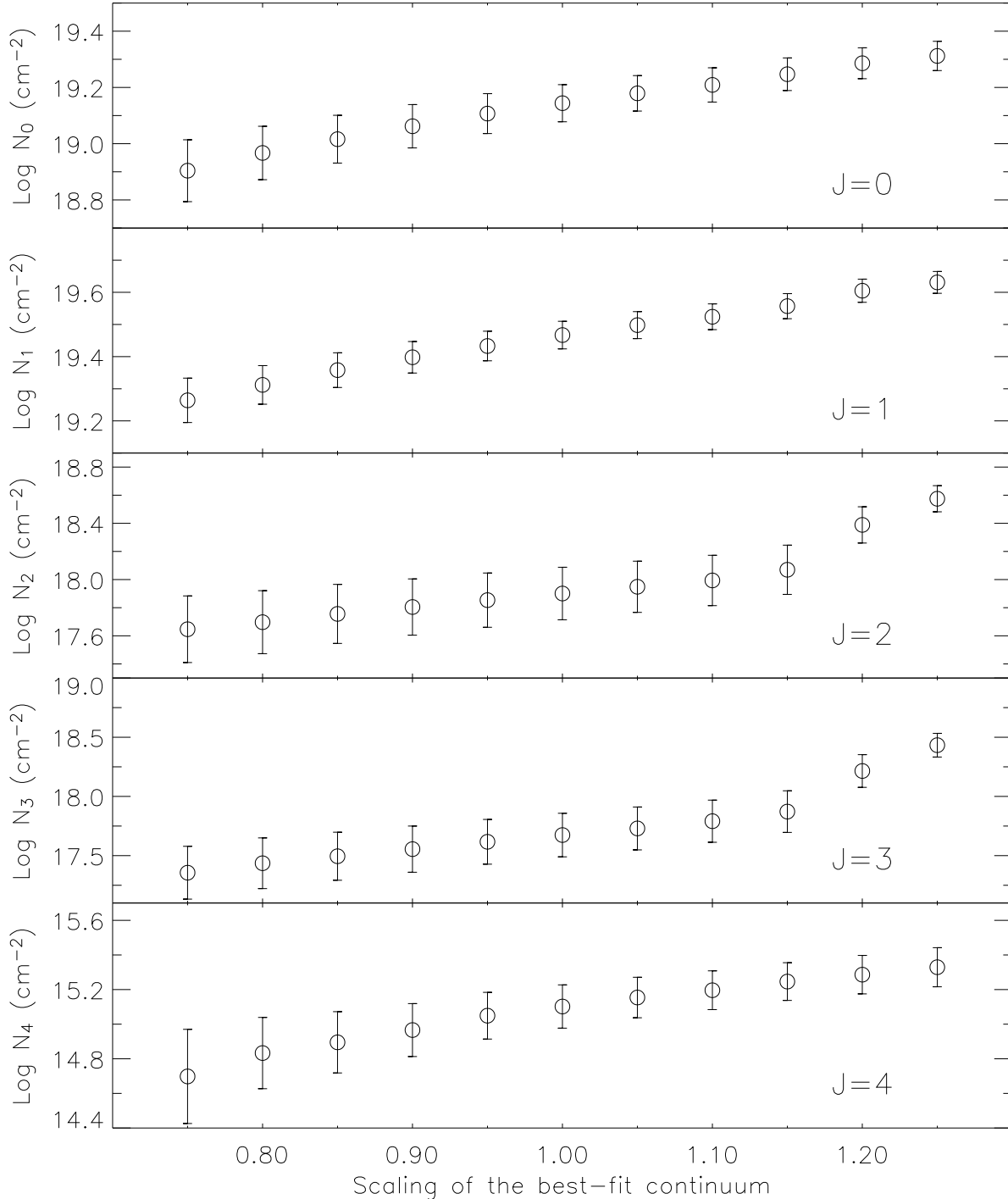


Fig. 5.— The effect of continuum fitting on the measured column densities of H_2 . The abscissa shows the scaling factor applied to the best-fit continuum shown in Fig. 1. The best-fit continuum corresponds to a scaling factor of 1.0.

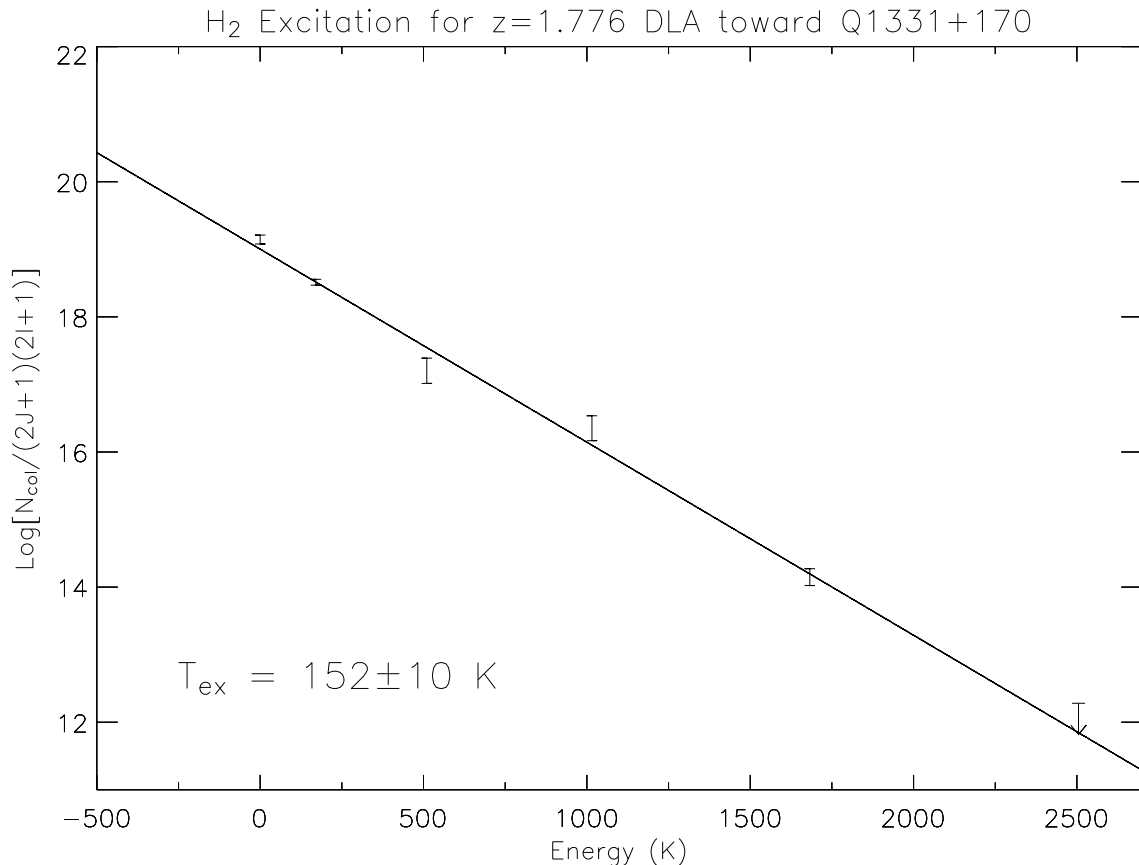


Fig. 6.— Distribution of molecular hydrogen at different J levels. The abscissa gives the relative energy for each J state relative to $J = 0$, expressed in units of Kelvin; the ordinate gives the column density divided by the degeneracy of the corresponding state, with 1σ errors. The population of H_2 at different J states can be fitted by a one-temperature Boltzmann distribution, with $T_{\text{ex}} \approx 152 \text{ K}$.

the kinetic temperature of the gas, while T_{ex} for high J states results from UV pumping (Spitzer *et al.* 1974). For the damped Ly α absorber of Q1331+170, a unique excitation temperature for all states from $J = 0$ to 4 indicates that the rotational populations of H₂ are probably dominated by collisional excitation in a gas with kinetic temperature around 150 K. Moreover, the local UV radiation field does not significantly populate the high J states of H₂ molecules. We quantify the UV radiation field below (see Sec. 4.1).

4. Discussion

4.1. UV radiation field

A simple analysis on the rate equation of the $J = 4$ state can yield an estimate of the UV photo-absorption rate of H₂. Collisions do not provide an important population source for $J \geq 4$ states (e.g. Browning *et al.* 2003), unless the gas phase temperature is comparable with or higher than $T \approx \frac{\epsilon_{J \geq 4} - \epsilon_0}{k} \gtrsim 1700$ K. However, such a high temperature can be excluded for the damped Ly α absorber toward Q1331+170, either by the distribution of H₂ at different J states (see Fig. 6), or by the observation of 21 cm absorption line (Wolfe & Davis 1979, Chengalur & Kanekar 2000).

Previous work shows that the $J = 4$ state is mainly populated by direct formation into this level and pumping from $J = 0$, while the dominant depopulation mechanism is spontaneous decay (e.g., Dalgarno & Wright 1972, Jura 1975). Assuming a steady state, these effects can be combined into the following equation

$$p_{4,0}R_{\text{abs}}n(\text{H}_2, J = 0) + 0.19R_{\text{dust}}n(\text{HI})n(\text{H}) = A_{42}n(\text{H}_2, J = 4), \quad (4)$$

where R_{abs} is the photo-absorption rate, $n(\text{HI})$ is the neutral hydrogen number density, $n(\text{H}) \approx n(\text{HI}) + 2n(\text{H}_2)$ is the total hydrogen number density, R_{dust} is the H₂ formation rate on the surface of dust grains, $p_{4,0} = 0.26$ is the UV pumping efficiency from $J = 0$ to $J = 4$ (Jura 1975), and $A_{42} = 2.75 \times 10^{-9} \text{ s}^{-1}$ is the spontaneous transition probability from $J = 4$ to $J = 2$ (Wolniewicz *et al.* 1998). For simplicity, we assume 19% of all H₂ formation results in the population at $J = 4$ (Jura 1975), although more recent work suggests that this fraction may vary for different types of dust grains (Takahashi & Uehara 2001).

The equilibrium between the formation and photo-dissociation of H₂ can be written as

$$R_{\text{dust}}n(\text{HI})n(\text{H}) \approx 0.11R_{\text{abs}}n(\text{H}_2), \quad (5)$$

where we assume that approximately 11% of photo-absorption leads to photo-dissociation (Jura 1974). Combining Eqn. 4 and 5, we get $R_{\text{abs}} = (7.6 \pm 2.4) \times 10^{-13} \text{ s}^{-1}$. We note that the

photo-absorption rate derived this way is independent of the neutral hydrogen density, since the relevant term $Rn(\text{HI})n(\text{H})$ cancels from Eqn. 4 and 5. Therefore R_{abs} is independent of the adopted H I column density (see Sec. 3.5).

The photo-absorption rate, R_{abs} derived above is based on the H_2 population at the $J = 4$ state. Since $J = 4$ lines are optically thin (see Sec. 3.3), the photo-absorption rate within the H_2 cloud should be approximately the same as that outside the cloud. Therefore R_{abs} is also characteristic of the UV background intensity in the absorber's environment. With this in mind, we use R_{abs} derived above to estimate the ambient UV radiation field at 1000 Å from the expression,

$$R_{\text{abs}} = 4.0 \times 10^{-10} S_{\text{shield}} \frac{J_{1000 \text{ \AA}}}{J_{1000 \text{ \AA}, \odot}} \text{ s}^{-1}, \quad (6)$$

where $J_{1000 \text{ \AA}, \odot} \approx 3.2 \times 10^{-20} \text{ ergs s}^{-1} \text{ cm}^{-2} \text{ Hz}^{-1} \text{ Sr}^{-1}$ is the UV intensity at 1000 Å in the solar vicinity (Hirashita & Ferrara 2005), and S_{shield} corrects for the the H_2 self-shielding and/or dust extinction. Since the $J = 4$ lines are optically thin, the self-shielding of H_2 can be reasonably ignored, and we estimate the importance of dust extinction following Hirashita & Ferrara (2005), i.e.

$$S_{\text{shield}} \approx \exp \left[-0.879 \kappa \left(\frac{N_{\text{HI}}}{10^{21} \text{ cm}^{-2}} \right) \right], \quad (7)$$

where κ is the dust-to-gas ratio, defined as the ratio of the extinction optical depth to neutral hydrogen column density in units of 10^{21} cm^{-2} (Pei *et al.* 1991). Vladilo (1998) showed that κ can be estimated by

$$\kappa = 1.7 \times 10^{[\text{Zn}/\text{H}]} (1 - 10^{[\text{Fe}/\text{Zn}]}). \quad (8)$$

Assuming that ZnII and FeII are the dominant ionization states for these two species, we adopt $[\text{Fe}/\text{H}] = -1.22$ and $[\text{Fe}/\text{Zn}] = -0.87$ for the Q1331+170 DLA from Prochaska & Wolfe (1999). This gives $\kappa \approx 0.088$, and therefore $S_{\text{shield}} \approx 0.89$, with our adopted H I column density (see Sec. 3.2). Inserting the above values into Eqn. 6, we get

$$\frac{J_{1000 \text{ \AA}}}{J_{1000 \text{ \AA}, \odot}} \approx (2.1 \pm 0.7) \times 10^{-3}, \quad (9)$$

i.e. the ambient UV radiation field of the H_2 cloud associated with DLA 1331+170 is about three orders of magnitude weaker than that in the Solar vicinity. Assuming the spectrum of the UV radiation field follows $J_{\nu} \propto \nu^{-0.5}$, we estimate the UV intensity at the Lyman limit as

$$J_{912 \text{ \AA}} \approx (7.1 \pm 2.3) \times 10^{-23} \text{ ergs s}^{-1} \text{ cm}^{-2} \text{ Hz}^{-1} \text{ Sr}^{-1}. \quad (10)$$

This value is consistent with the mean metagalactic UV background intensity of $J_{912 \text{ \AA}} \approx 7.6_{-3.0}^{+9.4} \times 10^{-23} \text{ ergs s}^{-1} \text{ cm}^{-2} \text{ Hz}^{-1} \text{ Sr}^{-1}$ at similar redshifts determined from proximity effect

in the Ly α forest (Scott *et al.* 2002), implying that the ambient UV radiation of the H₂ absorber may originate externally from the cloud. If instead the UV field is stellar in origin, $J_{912\text{ \AA}}^{\circ}$ would be lower than the metagalactic value, so our assumption of $J_{\nu} \propto \nu^{-0.5}$ gives a reasonable upper limit to the ionizing radiation field. Based on the above calculations, the existence of any significant internal source of UV emission is not allowed, suggesting negligible star formation activity associated with this H₂ absorber. Finally, we emphasize that our estimate of $J_{912\text{ \AA}}^{\circ}$ is based on the assumption of QSO-only spectral shape for the UV background intensity. This is a reasonable assumption if star-forming galaxies do not make significant contribution to the metagalactic UV radiation field (e.g. Leithere *et al.* 1995, Hurwitz *et al.* 1997, Deharveng *et al.* 2001, Giallongo *et al.* 2002, Fernández-Soto *et al.* 2003).

The ambient UV intensity for DLA 1331+170 is much smaller than that in other DLAs, which is usually close to the typical Galactic value (e.g. Ge & Bechtold 1997, Levshakov *et al.* 2002, Ledoux *et al.* 2002). Hirashita & Ferrara (2005) estimated that the probable range of radiation field is $0.5 \lesssim \log \left(\frac{J_{\text{912 \AA}}^{\circ}}{J_{1000\text{ \AA},\odot}^{\circ}} \right) \lesssim 1.5$, for a sample of DLAs which have been previously searched for H₂ absorption (Ledoux *et al.* 2003). The associated surface star formation rate (SFR) is $5 \times 10^{-3} \text{ M}_{\odot} \text{ yr}^{-1} \text{ kpc}^{-2} \lesssim \Sigma_{\text{SFR}} \lesssim 5 \times 10^{-2} \text{ M}_{\odot} \text{ yr}^{-1} \text{ kpc}^{-2}$ (Hirashita & Ferrara 2005, see also Wolfe *et al.* 2003a, 2003b). Also, we note that Reimers *et al.* (2003) reported the detection of H₂ associated with a sub-DLA system, with local UV radiation field inferred to be ~ 300 times stronger than the mean Galactic value. Although most DLAs may be associated with considerable on-going star formation, the DLA toward Q1331+170 at least represents a special system, which is in a stage either before the onset of considerable star formation, or after star forming activities have ceased.

For comparison, we note that the C II* 1336 \AA absorption feature is useful for probing the ambient UV intensity near 1500 \AA (Wolfe *et al.* 2003a, 2003b). Thus it is interesting to compare the UV radiation field inferred by C II* with that determined from H₂. Using the C II* absorption line as a diagnostic of the UV radiation field follows the idea that [CII]158 μm emission is the dominant coolant in DLAs, and is balanced by the grain photoelectric heating in a steady state. Since the grain photoelectric heating rate is proportional to the ambient UV intensity, a measurement of the strength of C II* 1336 \AA absorption provides an estimate of the UV radiation field at 1500 \AA . Following Wolfe *et al.* (2003a), we express the heating rate per H atom as

$$\Gamma = 10^{-24} \kappa \epsilon \left(\frac{J_{1500\text{ \AA}}^{\circ}}{10^{-19} \text{ ergs s}^{-1} \text{ cm}^{-2} \text{ Hz}^{-1} \text{ Sr}^{-1}} \right) \text{ ergs s}^{-1} \text{ H}^{-1}, \quad (11)$$

where $\kappa = 0.088$ is the dust-to-gas ratio determined from Eqn. 8, $\epsilon \approx 0.049$ is the heating efficiency (Bakes & Tielens 1994, Wolfire *et al.* 1995), and $J_{1500\text{ \AA}}^{\circ}$ is the UV intensity at

1500 Å. For the DLA towards Q1331+170, the C II* 1336 Å absorption line strength implies a cooling rate of $l_c \approx 2.24 \times 10^{-27} \text{ ergs s}^{-1} \text{ H}^{-1}$ (Wolfe *et al.* 2003a). Equating Γ and l_c implies $J_{1500 \text{ \AA}} \approx 5.4 \times 10^{-20} \text{ ergs cm}^{-2} \text{ s}^{-1} \text{ Hz}^{-1} \text{ Sr}^{-1}$, not too far from the mean Galactic value and much higher than the UV radiation field inferred from H₂ absorption. This discrepancy is not expected, since the large difference in the UV intensity determined from H₂ and C II* is difficult to be interpreted by any local sources of absorption. Note that H₂ and C II* absorption probe UV intensity near ~ 1000 Å and ~ 1500 Å, respectively, which are both above the Lyman limit. This indicates that photoionization of H I is not relevant. We also mentioned above that $J_{1000 \text{ \AA}} \circ$ determined from H₂ absorption is characteristic of the UV radiation field outside the H₂ cloud, therefore molecular hydrogen absorption in the Lyman and Werner bands does not account for the discrepancy either. However, the very low ambient UV intensity determined for the H₂ absorber is reasonable, otherwise the residual excitation temperature inferred from C I/C I* absorption would be far below the cosmic microwave background (CMB) temperature predicted by the standard cosmology (see Sec. 4.7).

4.2. The structure of the H₂ absorber

To study the structure of the H₂ cloud associated with the DLA of Q1331+170, we use CLOUDY (version c9400) to construct a grid of models with different total hydrogen number density $n(\text{H}) \approx n(\text{HI}) + 2n(\text{H}_2)$, and examine which model provides the best match with the observed H₂ column density. We adopt a metallicity of [Zn/H] = −1.22 (Prochaska & Wolfe 1999) for all the elements in the absorber. To take into account differential dust depletion, we determine the dust-to-gas ratio κ according to Eqn. 8. The ambient UV intensity is characterized by the metagalactic UV radiation field, assuming a QSO-like spectral shape, as implied by results in Sec. 4.1. For simplicity, we assume plane parallel geometry with a uniform total hydrogen number density. The cloud is illuminated from both sides in our model, and we run the calculation until the neutral hydrogen column density reaches the observed value of $N(\text{HI}) = 1.5 \times 10^{21} \text{ cm}^{-2}$.

The model with a total hydrogen number density, $n(\text{H}) \approx n(\text{HI}) + 2n(\text{H}_2) \approx 0.22$, gives the best match to the observed H₂ fraction for the $z = 1.7765$ DLA system. We show in Fig. 7.1 the thermal structure of the cloud, with the electron temperature determined from the balance between cooling and heating. In Fig. 7.2, we give the structure of the cloud traced by H I, H II, H₂ and e . We find that the neutral hydrogen number density remains almost constant from the boundary deep into the central region. The molecular hydrogen fraction is very low in an outer shell with a thickness of ~ 46 pc, and increases sharply from $< 10^{-5}$

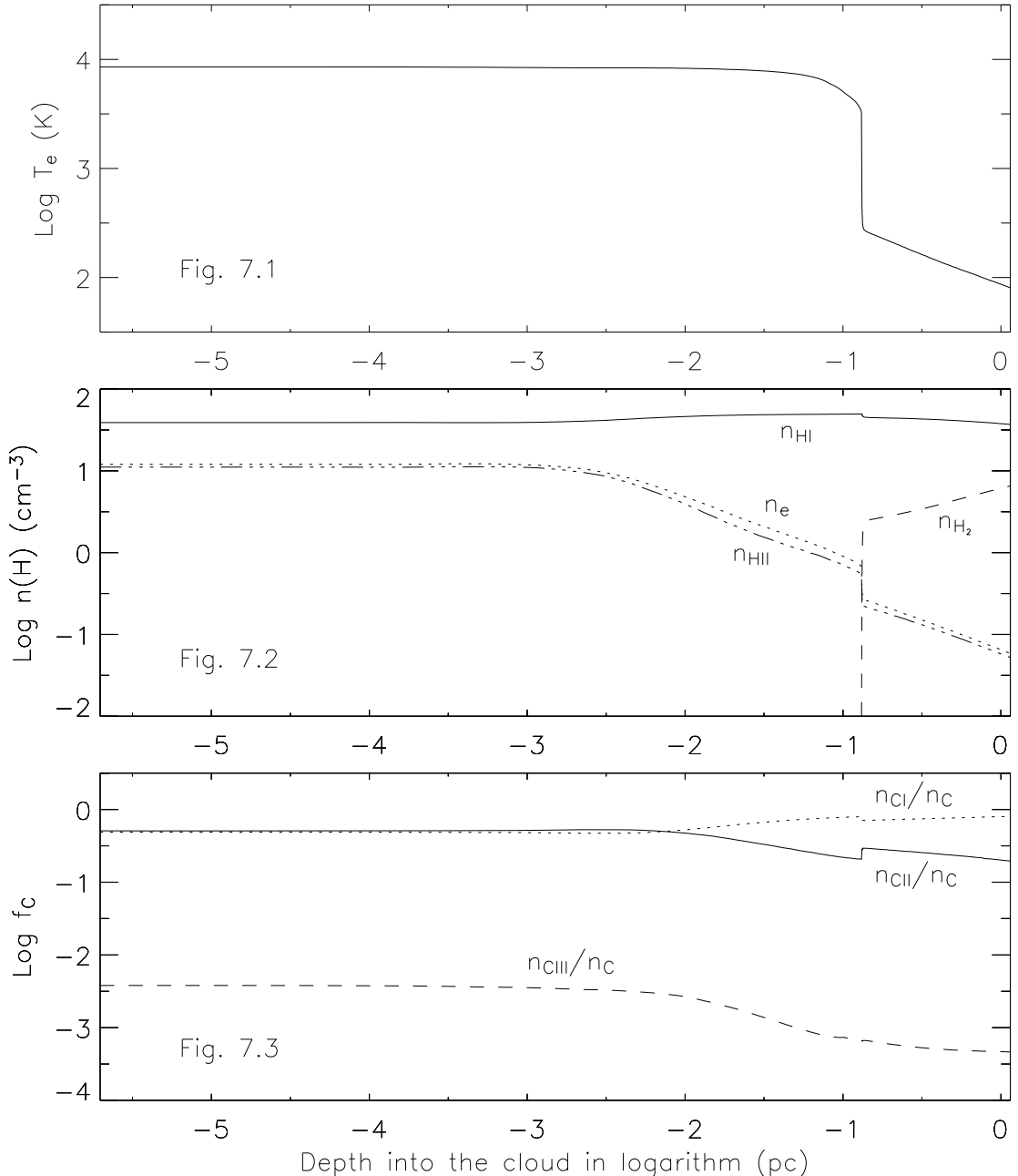


Fig. 7.— Model calculations of the thermal and ionization structure of the H_2 cloud (see Sec. 4.2). The electron temperature (upper panel), the number densities of H I , H II , H_2 , electrons (middle panel), and the fraction of different species of carbon (lower panel) are each plotted as a function of the depth into the cloud. Note that only half of the cloud is shown in the figure (~ 1.2 kpc).

in the shell to $\sim 10^{-2}$ in the center. We note that the outer shell is very thin, compared with the depth of the center region (~ 1.2 kpc). The $\frac{n(p)}{n(HI)}$ ratio decreases monotonically with the depth into the cloud, and the metagalactic UV radiation field does produce some fraction of ionization in the outer shell of the cloud ($\frac{n(p)}{n(HI)} \approx 20\%$). Fig. 7.1 shows that the electron temperature in the center H₂ core is much lower than that in the outer shell, and has a mean value of $T_e \approx 140$ K, in broad agreement with the excitation temperature determined in Sec. 3.4.

Fig. 7.3 shows the ionization structure of carbon for our model. The dominant ionization state is C I and C II. Although the ambient UV radiation results in some fraction of C III before it's shielded by molecular hydrogen, the model calculation shows that the column density of highly ionized carbon species (e.g. C IV) is completely negligible.

Compared with observations, these results suggest that the Q1331+170 absorber has multiple velocity components with different carbon ionization. First, the observed value of $N_{CII}/N_{CI} \approx 2647$ for Q1331+170 (Liszt 2002) is much larger than the model prediction of ~ 3.5 for the H₂ cloud. Second, there is strong CIV absorption associated with this damped Ly α system, with $N(CIV) > 10^{15} \text{ cm}^{-2}$ (Prochaska & Wolfe 1999). Therefore the bulk of the observed C II and C IV are associated with other components, either in a warm/hot phase, or embedded in a UV radiation field much stronger than that derived for the H₂ absorber (see also Sec. 4.1).

Dessauges-Zavadsky *et al.* (2004) reported multiple velocity components associated with the DLA of Q1331+170, and they did find non-negligible differences between the component structure of low-ion transitions and that of intermediate-ion transitions. We note that the H₂ cloud identified in our spectrum is different from the five intermediate-ion velocity components by 56 km s^{-1} , 28 km s^{-1} , 15 km s^{-1} , -15 km s^{-1} , and -34 km s^{-1} in the rest frame, respectively. On the other hand, it agrees with one low-ion component with detected C I absorption, with a velocity difference of only 1.6 km s^{-1} in the rest frame. Songaila *et al.* (1994) reported two C I absorption features associated with the same system, which are different from the H₂ cloud by 1.4 km s^{-1} and 19 km s^{-1} in the rest frame. The 1σ uncertainty is 1.2 km s^{-1} , caused by wavelength calibration and line centroiding (see Sec. 3.2), and therefore we conclude that the molecular hydrogen absorption identified in our STIS spectrum is consistent with one low-ion component reported by Dessauges-Zavadsky *et al.* (2004), as well as one C I component reported by Songaila *et al.* (1994). This is as expected since H₂ tends to be co-spatial with neutral carbon and/or other low ion species.

4.3. Mass and dynamical state of the H₂ cloud

Based on the model shown in Fig. 7.2, we estimate the mass of the entire cloud as $M \approx 1.36 \times \frac{4}{3}\pi R^3[n(\text{HI})m_{\text{H}} + n(\text{H}_2)m_{\text{H}_2}] \approx 6.5 \times 10^7 \text{ M}_{\odot}$, where we take $R \approx 1.2 \text{ kpc}$, $n(\text{HI}) \approx 0.17 \text{ cm}^{-3}$, $n(\text{H}_2) \approx 0.05 \text{ cm}^{-3}$, and the factor of 1.36 corrects for the abundance of helium (Dickman 1978). We refer to this mass as M_{LTE} , since our model is constructed based on the assumption of local thermodynamic equilibrium. Here we have ignored the small mass fraction contributed by H II. We also assume spherical geometry for the absorbing region.

The masses of giant molecular clouds (GMCs) have been measured for the Milky Way (e.g. Solomon *et al.* 1987, Digel *et al.* 1996, Heyer *et al.* 2001), and nearby galaxies such as LMC (Mizuno *et al.* 2001a), SMC (Mizuno *et al.* 2001b), and M33 (Engargiola *et al.* 2003). These masses are either determined based on the assumption of self-gravitational equilibrium, i.e. virial mass, M_{vir} , or determined by adopting a constant CO-to-H₂ conversion factor and then integrating the H₂ column density over the projected area of the cloud, i.e. CO luminosity mass, M_{CO} . In all cases, the mass spectrum of GMCs has been found to follow approximately a power law, with the power index ranging from ~ -1.8 for the Milky Way (Heyer *et al.* 2001) to ~ -2.6 for M33 (Engargiola *et al.* 2003). The mass of the H₂ cloud associated with the DLA towards Q1331+170 is much larger than the values determined for most GMCs in either the Milky Way or nearby galaxies. For example, it is almost two orders of magnitude greater than the value of $7 \times 10^5 \text{ M}_{\odot}$ for the most massive GMC in M33 (Engargiola *et al.* 2003). Similarly, if we adopt the GMC mass spectrum of $\frac{dM}{dN} \propto M^{-1.8}$ in the Milky Way, and take the limiting CO luminosity of $138 \text{ K km s}^{-1} \text{ pc}^2$, corresponding to 566 M_{\odot} (Heyer *et al.* 2001), we find that the fraction of GMCs with masses greater than $6.5 \times 10^7 \text{ M}_{\odot}$ (the value derived for the H₂ cloud associated with DLA 1331+170) is only 9×10^{-5} in the Milky Way. This may simply result from our assumption of spherical symmetry, or from the fact that the spectral resolution of our STIS spectrum is not high enough to resolve individual molecular clouds in velocity space along the line-of-sight. Note that the typical velocity dispersions measured for Galactic GMCs peak at $\sigma_v \sim 1 \text{ km s}^{-1}$ (Heyer *et al.* 2001), much smaller than the spectral resolution of $\sim 10 \text{ km s}^{-1}$ for our spectrum and the b -parameter of $\sim 20 \text{ km s}^{-1}$ for the H I gas in DLA 1331+170. The total H₂ mass inside a 2 kpc galactocentric radius has been determined for a sample of 17 nearby galaxies (Paglione *et al.* 2001), based on the observed CO emission and a standard CO-to-H₂ conversion factor of $1.6 \times 10^{20} \text{ cm}^{-2} \text{ K}^{-1} \text{ km}^{-1} \text{ s}$. These masses range from $1.6 \times 10^8 \text{ M}_{\odot}$ to $2.8 \times 10^9 \text{ M}_{\odot}$, much larger than our value of $6.5 \times 10^7 \text{ M}_{\odot}$. This is consistent with the general deficiency of molecular hydrogen in damped Ly α systems, especially when considering that the DLA towards Q1331+170 presents the largest H₂ fraction in all high-z DLAs.

It is interesting to compare the mass derived above, i.e. M_{LTE} , with the mass predicted

by self-gravitational equilibrium, i.e. M_{vir} . We estimate the virial mass by

$$M_{\text{vir}} \approx K \frac{\sigma_v^2 R}{G} = 9.6 \times 10^8 M_{\odot}. \quad (12)$$

Here σ_v is the one-dimensional velocity dispersion which we approximate as the b -parameter determined in Sec. 3.2, $R \approx 1.2$ kpc is the size of the cloud (see Sec. 4.2), G is the gravitational constant, and K is a dimensionless factor of order unity that depends on the geometry as well as the density profile of the cloud. We adopt $K \approx 8.7$ from Solomon *et al.* (1987). Correspondingly, the gravitational parameter, $\alpha_G = \frac{M_{\text{vir}}}{M_{\text{LTE}}} \approx 14$, indicating that the H_2 cloud can not be bound by self-gravity. This is contrary to the situation for most Galactic GMCs, of which the self-gravitational equilibrium state has long been established (e.g. Solomon *et al.* 1987). More recently, Heyer *et al.* (2001) found that the dynamical state of Galactic GMCs varies with the cloud mass, in that $M_{\text{CO}} > 10^4 M_{\odot}$ clouds are bound by self-gravity. One possible interpretation to the large α_G value is that the H_2 cloud towards Q1331+170 is in hydrostatic equilibrium, i.e. bound by the pressure of an external medium. Here we emphasize that the above result is subject to uncertainties due to the unknown geometry and density profile of the cloud.

4.4. Molecular hydrogen fraction

In Sec. 3.2, we derived a molecular hydrogen fraction of $f_{\text{H}_2} = (5.6 \pm 0.7)\%$, for the $z = 1.7765$ DLA toward Q1331+170, which is the largest value reported so far in any redshifted damped Ly α absorber. The large value of f_{H_2} is consistent with the relatively high dust abundance for this system. In Sec. 4.2, we derived the dust-to-gas ratio to be $\tilde{k} \approx 0.088$. Ledoux *et al.* (2003) showed that there exists a threshold at $\tilde{k} \approx 0.03$ above which the molecular hydrogen fraction tends to be large ($f_{\text{H}_2} > 10^{-4}$). Moreover, the model described in Sec. 4.2 suggests a low gas phase temperature, which is also supported by the distribution of H_2 at different J states. The low kinetic temperature is representative of a cold neutral medium (CNM) phase, in which efficient formation of H_2 molecules onto dust grains is possible. Third, the ambient UV radiation field of the H_2 cloud is extremely low, implying that destruction of H_2 molecules by photo-dissociation is ineffective.

It is interesting to compare the damped Ly α absorber toward Q1331+170 with other high-redshift damped systems. In Table 4, we compiled data for all the 42 DLAs which have been searched for molecular hydrogen absorption, including Q1331+170. In the upper panel of Fig. 8, we show the distribution of damped Ly α absorbers with respect to neutral hydrogen column density and molecular hydrogen fraction. The figure clearly shows the bi-modal distribution of DLAs, i.e. for a certain value of N_{HI} , the molecular hydrogen fraction

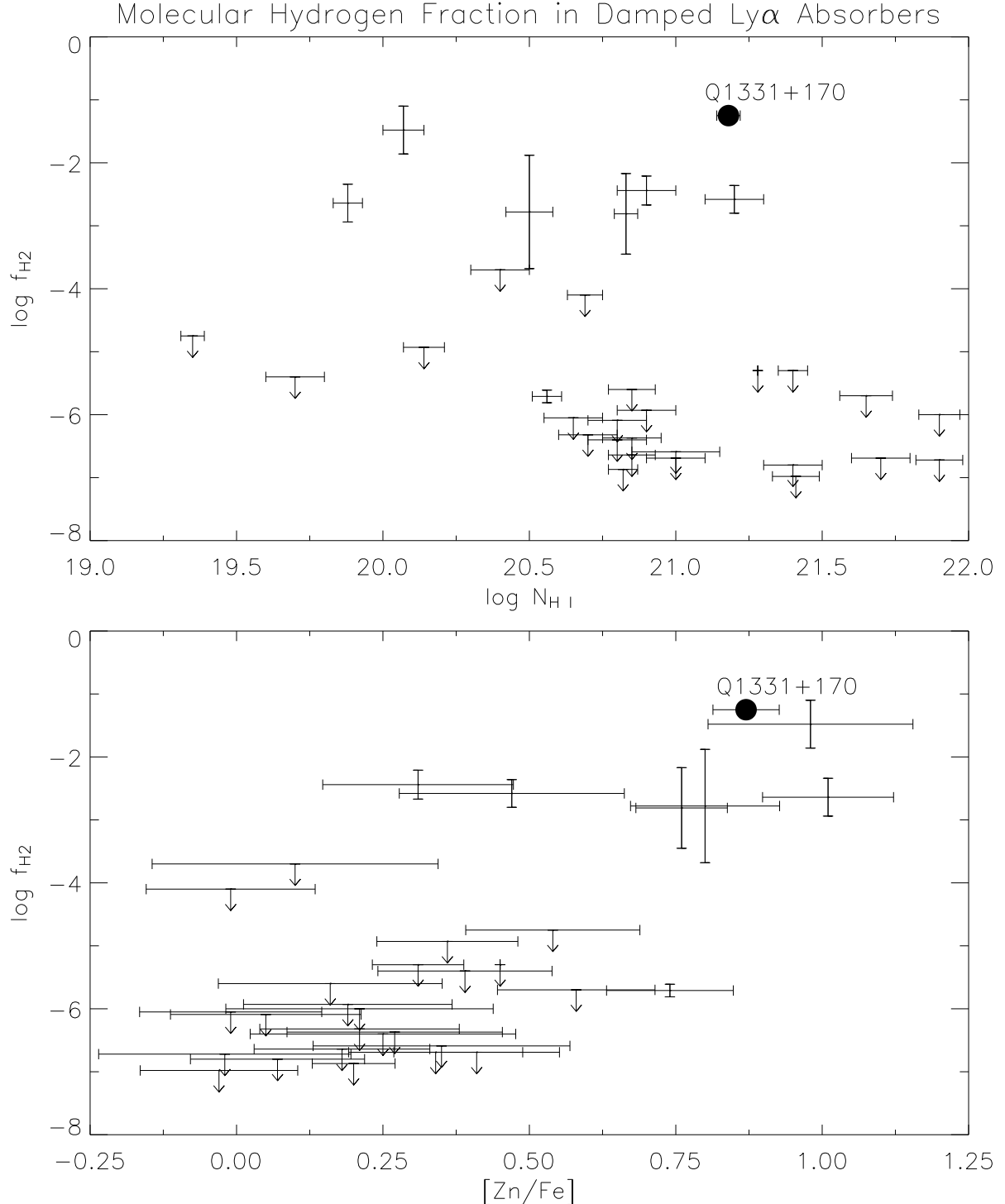


Fig. 8.— Relation between molecular hydrogen fraction f_{H_2} and neutral hydrogen column density (top) and dust abundance (bottom) for damped Ly α absorbers. The upper panel shows the bi-model distribution of high-redshift DLAs, which can be understood as a result of self-shielding of molecular hydrogen. The lower panel shows a strong correlation between the molecular hydrogen fraction and the dust abundance, characterized by the ratio of undepleted elements ($\text{Zn} + \text{Sc}$) to depleted elements ($\text{Fe} + \text{Cr}$). Data points taken from Table 4. In both

of the absorber can be either as large as $\sim 10^{-1} - 10^{-3}$, or smaller than the detection limit ($\sim 10^{-5} - 10^{-7}$). This can be interpreted by the self-shielding effect of molecular hydrogen: once molecular hydrogen begins to form, it shields itself from subsequent photodissociation by UV photons, and thus the molecular hydrogen fraction increases significantly (see also Ge & Bechtold 1999). The lower panel of Fig. 8 shows the relation between the molecular hydrogen fraction and the dust abundance in the same system. The dust abundance is characterized by the column density ratio of undepleted element to depleted element. For element which is not depleted, we take Zn as a representative, whereas when Zn is not available in the literature, we adopt S instead. The element which is depleted to the dust grain is represented by Fe, and when Fe abundance has not been measured, we take Cr instead. The lower panel of Fig. 8 shows a strong correlation between the dust abundance and the molecular hydrogen fraction, similar to previous results (e.g. Ledoux *et al.* 2003). Kendall’s τ test shows the correlation is present at $> 99.9\%$ confidence level. In Fig. 8, the damped Ly α absorber toward Q1331+170 is indicated by a solid circle.

4.5. Dust extinction

The reddening of QSOs with intervening DLAs compared with non-DLA QSOs has been detected and quoted as evidence for the presence of dust in DLAs (e.g. Fall & Pei 1989, Pei *et al.* 1991). More recently, Murphy & Liske (2004) showed that there is no evidence for the dust reddening of QSOs with DLAs, based on a much larger sample selected from the Sloan Digital Sky Survey Data Release 2 (SDSS DR2) catalog. However, since the SDSS main QSO sample is largely color-selected (Richards *et al.* 2002), the non-detection by Murphy & Liske (2004) may simply be a selection effect against heavily reddened objects. In this section, we estimate the dust reddening of Q1331+170, due to the damped Ly α absorber at $z \approx 1.7765$, and we also compare the reddening of QSOs for which the intervening DLAs have different molecular hydrogen fractions.

Similar to Pei (1992), we calculate the color excess, $E_{\text{B}-\text{V}}$, of Q1331+170 by

$$E_{\text{B}-\text{V}} = 1.086 \frac{\kappa}{1 + R_V} \left(\frac{N_{\text{HI}}}{10^{21} \text{ cm}^{-2}} \right), \quad (13)$$

where $\kappa \approx 0.088$ for DLA 1331+170 is the dust-to-gas ratio determined from Eqn. 8, and R_V is the ratio of total-to-selective extinction, which depends on the exact extinction curve adopted in our calculation. If we assume the SMC extinction curve, then $R_V = 2.93$ (Pei 1992) and $E_{\text{B}-\text{V}} \approx 0.037 \pm 0.005$. We also calculate $E_{\text{B}-\text{V}}$ by adopting the mean $N_{\text{HI}}/E_{\text{B}-\text{V}}$ values of 36.1 ± 3.3 based on the new determination of the SMC extinction curve (for the SMC bar sample) by Gordon *et al.* (2003), where N_{HI} is in units of 10^{21} cm^{-2} . This gives

the same value of E_{B-V} within 1σ errors. There are two reasons for adopting the SMC extinction curve. First, the DLAs are believed to be in an early stage of chemical evolution, which is well characterized by the SMC extinction curve (e.g. Pei 1992). Second, DLAs show no evidence for the 2175 Å dust feature observed in either Galactic or LMC extinction curve (e.g. Fall & Pei 1989, but see Malhotra 1997 which reported the detection of this feature based on a sample of Mg II absorbers).

In column 7 of Table 4, we give E_{B-V} for each QSO of which the intervening DLA has previous measurements of both depleted and undepleted metal absorption. These values are calculated similar to the Q1331+170 case. However, we use a different normalization when estimating the dust-to-gas ratio by Eqn. 8, depending on the types of depleted/undepleted elements adopted in the calculation (see Table 1 of Vladilo 1998). For several QSOs with more than one intervening DLAs (Q0013-004, Q0405-443, Q0841+129 and Q2059-360), we only list in Table 4 E_{B-V} contributed by individual absorbers, which does not represent the total extinction towards the background QSO. Fig. 9 presents the distribution of E_{B-V} for DLAs with firm H₂ detections (solid line) as well as the distribution for DLAs for which only upper limits of f_{H_2} have been put (dashed line). The extinction for Q1331+170 is marked with an arrow. The two distributions in Fig. 9 are different at 99.8% confidence level, based on Kolmogorov-Smirnov test. Specifically, the sub-sample of DLAs with firm H₂ detections shows more extinction compared with other DLAs. The mean color excess for absorbers with firm H₂ detections is $\langle E_{B-V} \rangle = 0.038 \pm 0.001$, significantly greater than the value of $\langle E_{B-V} \rangle = 0.014 \pm 0.001$ for cases in which only upper limits of f_{H_2} have been reported. Whereas only 12.5% of DLAs with firm H₂ detections have E_{B-V} smaller than 0.01, this fraction is as large as 75% for other DLAs. We have also examined the relation between E_{B-V} and f_{H_2} , but no significant correlation has been found.

The intrinsic QSO continuum in the UV/optical band is reddened by the dust extinction due to an intervening DLA. Assuming the QSO continuum follows $F_\nu \propto \nu^{-\alpha}$ or equivalently $F_\lambda \propto \lambda^{\alpha-2}$, we get $\alpha \approx 4.1$ by fitting a power law to the dereddened continuum (between 2600 Å and 3000 Å) of the QSO, Q1331+170, while $\alpha = 4.2$ for the observed, reddened continuum adopted in Sec. 2. For dereddening of the Galactic extinction, we use the extinction map of Schlegel *et al.* (1998). For reddening of the intervening damped Ly α absorber at $z \approx 1.7765$, we adopt the FM parametrization (Fitzpatrick & Massa 1990) determined for the SMC bar sample (Gordon *et al.* 2003). The observed spectrum has been shifted to the rest frame of the absorber before dereddening. The value of 4.1 for the dereddened spectral slope indicates an extremely red intrinsic spectrum below the rest frame wavelength of ~ 970 Å for Q1331+170.

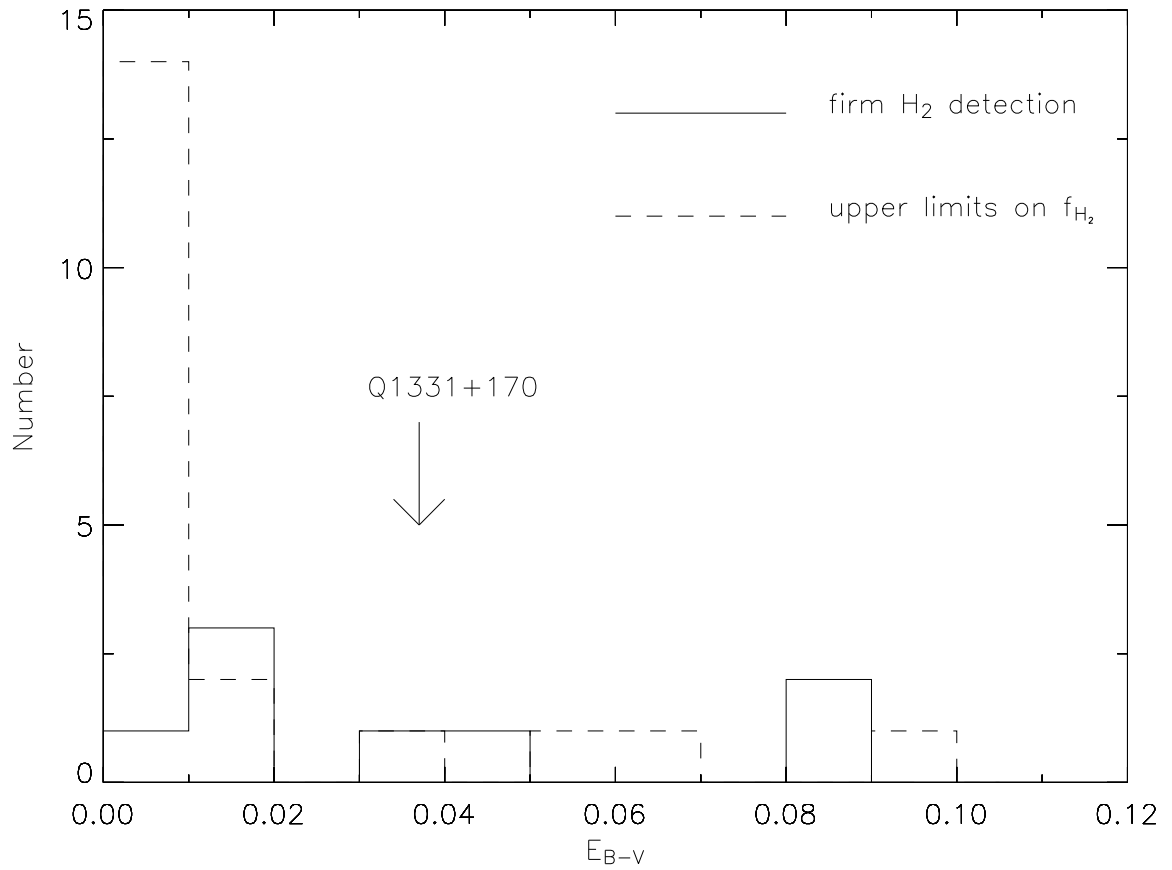


Fig. 9.— The distribution of E_{B-V} for damped Ly α absorbers which have been searched for molecular hydrogen absorption. The solid line represents the histogram for the eight DLAs with firm H_2 detections, whereas the dashed line represents the histogram for other DLAs for which only upper limits of f_{H_2} have been put. The two distributions are clearly different, in the sense that DLAs with H_2 detections show significantly more extinction.

4.6. CO-to-H₂ ratio

According to our model calculations in Sec. 4.2, the predicted CO column density is $6.7 \times 10^{10} \text{ cm}^{-2}$. This is consistent with the observed 2σ upper limit of $N_{\text{CO}} < 1.1 \times 10^{13} \text{ cm}^{-2}$ (Levshakov *et al.* 1988), determined from UV absorption lines of CO ($A^1\Pi \rightarrow X^1\Sigma^1$). Adopting the total molecular hydrogen column density in Table 3, we obtained the observed CO-to-H₂ column density ratio of $\frac{N_{\text{CO}}}{N_{\text{H}_2}} < 2.5 \times 10^{-7}$.

The upper limit of the CO-to-H₂ column density ratio for DLA 1331+170 is similar to the typical value of CO-to-H₂ measured from UV absorption of CO in Galactic diffuse clouds, where the effects of CO self-shielding are not important (e.g. Crenny & Federman 2004). For dense molecular clouds in the Milky Way, the CO/H₂ conversion factor is given in terms of the quantity $\frac{I_{\text{CO}}}{N_{\text{H}_2}}$, where I_{CO} is related to the antenna temperature T_A directly measurable from millimeter CO emission lines (e.g. Strong *et al.* 1988). $\frac{I_{\text{CO}}}{N_{\text{H}_2}}$ usually does not provide information on the corresponding column density ratio, since the profiles of the optically thick CO lines give the velocity width of molecular clouds rather than the CO column densities. The ratio of CO to H₂ column densities in typical dense molecular clouds in the Milky Way is $\sim 10^{-4}$, three orders of magnitude higher than the upper limit determined for the DLA toward Q1331+170 (e.g. Frerking *et al.* 1992, Lacy *et al.* 1994). This could be associated with the relatively low number density of the H₂ cloud (see Sec. 4.2), since the CO abundance is controlled by collisional reactions involved with various species, including O, C, H₂, CH and CH₂ (e.g. Tielens & Hollenbach 1985).

4.7. Measurement of CMB Temperature at $z = 1.77654$

Songaila *et al.* (1994) reported the detection of C I/C I* absorption features associated with a velocity component at $z = 1.77654$. As described in Sec. 4.2, the redshift of this component agrees with the redshift of the H₂ absorber identified in our spectrum at 1.2σ . Therefore, the C I and H₂ probably arises in the same gas cloud. Theoretically, C I and H₂ tend to be co-spatial as well (Ge *et al.* 1997, 2001). With the physical parameters determined in Sec. 4.1 and 4.2, we can estimate the local contribution to the C I excitation in this system and then put constraints on the CMB temperature at the absorber's redshift. The equilibrium between the population and de-population of the C I 3P_0 and 3P_1 fine structure can be written as

$$N_0(B_{01}I_\nu + \Gamma_{01} + \sum_j R_{01}^j n_j) = N_1(A_{10} + B_{10}I_\nu + \Gamma_{10} + \sum_j R_{10}^j n_j), \quad (14)$$

where R_{01} and R_{10} are collisional excitation and de-excitation rates, with j representing different collision partners (H, He, e , p , or H_2), Γ_{01} and Γ_{10} are UV pumping rates, $A_{10} = 7.93 \times 10^{-8} \text{ s}^{-1}$ is the probability of the C I fine structure transition ${}^3P_1 \rightarrow {}^3P_0$ (Bahcall & Wolf 1968). $B_{01}I_\nu$ and $B_{10}I_\nu$ represent excitation or de-excitation due to the absorption of ambient microwave photons, which can be expressed as

$$B_{01}I_\nu = 3B_{10}I_\nu = \frac{2.38 \times 10^{-7}}{\exp(23.6 \text{ K}/T_{\text{ex}}) - 1} \text{ s}^{-1}. \quad (15)$$

The collisional rates, R_{01}^j and R_{10}^j are taken from Launay & Roueff (1977), Johnson *et al.* (1987), Roueff & Le Bourlot (1990), Staemmler & Flower (1991), and Schröder *et al.* (1991), and are related through the Milne relation,

$$R_{10}^j = \frac{1}{3}R_{01}^j \exp(23.6 \text{ K}/T_{\text{K}}). \quad (16)$$

We take number densities of different species from the model described in Sec. 4.2. The various collision terms are calculated to be $R_{01}^{\text{HI}}n(\text{HI}) = 8.6 \times 10^{-10} \text{ s}^{-1}$, $R_{01}^{\text{He}}n(\text{He}) = 3.3 \times 10^{-13} \text{ s}^{-1}$, $R_{01}^{\text{H}_2}n(\text{H}_2) = 4.2 \times 10^{-13} \text{ s}^{-1}$, $R_{01}^{\text{p}}n(\text{p}) = 2.3 \times 10^{-12} \text{ s}^{-1}$, and $R_{01}^{\text{e}}n(\text{e}) = 1.4 \times 10^{-12} \text{ s}^{-1}$, assuming a kinetic temperature of 152 K. We determine the UV pumping rates for C I by scaling from the mean Galactic values (e.g. Ge *et al.* 1997), and get $\Gamma_{01} = 8.7 \times 10^{-13} \text{ s}^{-1}$ and $\Gamma_{10} = 2.8 \times 10^{-13} \text{ s}^{-1}$. Inserting these values into Eqn. 14 and 15, and taking $\frac{N({}^3P_1)}{N({}^3P_0)} = 0.125 \pm 0.042$ from Songaila *et al.* (1994), we get $T_{\text{ex}} = (7.2 \pm 0.8) \text{ K}$ at $z = 1.77654$. Note that the uncertainty in the calculated T_{ex} is associated with the errors in the measured C I/C I* column densities. The excitation temperature, T_{ex} , calculated above is consistent with the predicted CMB temperature of $2.725 \times (1 + z) = 7.566 \text{ K}$ at $z = 1.77654$, within 1σ .

5. Conclusions

The main results of this paper are summarized as follows:

1. Using the NUV spectrum with spectral resolution of $\sim 10 \text{ km s}^{-1}$ obtained with the E230M grating of HST/STIS, we detected strong molecular hydrogen absorption associated with the $z = 1.7765$ damped Ly α system toward Q1331+170. The total H_2 column density is $N_{\text{H}_2} = (4.45 \pm 0.36) \times 10^{19} \text{ cm}^{-2}$, determined from simultaneous Voigt profile fitting of 26 H_2 lines.

2. The molecular hydrogen fraction was determined to be $f_{\text{H}_2} = \frac{2N_{\text{H}_2}}{N_{\text{HI}} + 2N_{\text{H}_2}} = (5.6 \pm 0.7)\%$, which is the largest value reported so far in any redshifted damped Ly α system. This is a

combined effect of a relatively high dust-to-gas ratio, a low gas temperature, and an extremely low ambient UV radiation field.

3. We detect rotationally excited transitions of H₂, with $J = 0 - 4$. The relative column densities of the $J = 0, 1, 2, 3, 4$ states can be fit with a single temperature of $T_{\text{ex}} = 152 \pm 10$ K. This suggests that the derived excitation temperature represents the kinetic temperature of the gas, and that photo-excitation is negligible.

4. The photo-absorption rate was estimated to be $R_{\text{abs}} = (7.6 \pm 2.4) \times 10^{-13} \text{ s}^{-1}$, corresponding to an ambient UV radiation field of $J_{912\text{A}} \approx 7 \times 10^{-23} \text{ ergs s}^{-1} \text{ cm}^{-2} \text{ Hz}^{-1} \text{ Sr}^{-1}$. This is comparable with the metagalactic UV background intensity at the same redshift, and implies an extremely low star-formation rate in the DLA environment.

5. We constructed a simple model to describe the structure of the H₂ absorber, with a best-fit total hydrogen number density of $n_{\text{H}} \approx 0.2 \text{ cm}^{-3}$ and an electron temperature of $T_{\text{e}} \approx 140$ K. The total mass of the model cloud is $\sim 6.5 \times 10^7 M_{\odot}$, greater than masses of most GMCs in the Milky Way and nearby galaxies. We also find that this mass is considerably smaller than the virial mass of the cloud, indicating that the H₂ cloud is not in a state of self-gravitational equilibrium. Our model is consistent with the population of H₂ at different J states, as well as the observational upper limit put on the CO column density. The observed CO-to-H₂ column density ratio is $\frac{N_{\text{CO}}}{N_{\text{H}_2}} < 2.5 \times 10^{-7}$, characteristic of the typical value measured for diffuse molecular clouds in the Galactic ISM.

6. Adopting the SMC-like extinction curve, we calculate the extinction of Q1331+170 to be $E_{\text{B-V}} = 0.037 \pm 0.005$, due to the intervening damped Ly α absorber at $z \approx 1.7765$. We also find that the extinction of QSOs by foreground DLAs with firm H₂ detections is considerably greater than those for which only upper limits of f_{H_2} have been put.

7. The redshift of the H₂ absorber identified in our spectrum is consistent with a C I/C I* absorber reported by Songaila *et al.* (1994). We calculated the local contribution to C I excitation, including UV pumping and collisions. The residual excitation temperature was determined to be $T_{\text{ex}} = (7.2 \pm 0.8)$ K, consistent with the predicted T_{CMB} of 7.566 K at $z = 1.77654$.

We are grateful to R.I. Thompson, D.J. Eisenstein, X. Fan, D. Welty, J. Black, R. Davé, J. Bieging and the anonymous referee for their suggestions, which have greatly improved this work. We also thank R.F. Carswell and G. Ferland for making the Voigt profile fitting program VPFIT and the photoionization code CLOUDY publicly available. This work is based on observations made with the NASA/ESA *Hubble Space Telescope*, obtained at the *Space Telescope Science Institute*, which is operated by the *Association of Universities for*

Research in Astronomy, Inc., under NASA contract NAS 5-26555. These observations were supported by NASA through Grants HST-GO-09172.01 and HST-GO-07271.01 from the *Space Telescope Science Institute*.

REFERENCES

Abgrall, H., Roueff, E., Launay, F., Roncin, J.Y., & Subtil, J.L., 1993a, A&AS, 101, 273

Abgrall, H., Roueff, E., Launay, F., Roncin, J.Y., & Subtil, J.L., 1993b, A&AS, 101, 323

Bahcall, J.N. & Wolf, R.A., 1968, ApJ, 152, 701

Bahcall, J.N., Joss, P.C., & Lynds, R., 1973, ApJ, 182, L95

Bakes, E.L.O., & Tielens, A.G.G.M., 1994, ApJ, 427, 822

Baldwin, J.A., Burbidge, E.M., Hazard, C., Murdoch, H.S., Robinson, L.B., & Wampler, E.J., 1973, ApJ, 185, 739

Black, J.H., Chaffee, F.H.J., & Foltz, C.B., 1987, ApJ, 317, 442

Browning, M.K., Tumlinson, J., & Shull, J.M., 2003, ApJ, 582, 810

Carswell, R.F., Hilliard, R.L., Strittmatter, P.A., Taylor, D.J., & Weymann, R.J., 1975, ApJ, 196, 351

Cauzaux, S., & Tielens, A.G.G.M., 2002, ApJ, 575, L29

Centurión, M., Molero, P., Vladilo, G., Péroux, C., Levshakov, S.A., & D'Odorico, V., 2003, A&A, 403, 55

Chaffee, F.H.J., Foltz, C.B., & Black, J.H., 1988, ApJ, 335, 584

Chengalur, J.N., & Kanekar, N., 2000, MNRAS, 318, 303

Crenny, T., & Federman, S.R., 2004, ApJ, 605, 278

Curran, S.J., Webb, J.K., Murphy, M.T., & Carswell, R.F., 2004, MNRAS, 351, 24

Dalgarno, A., & Wright, E.L., 1972, ApJ, 174, L49

Deharveng, J.M., Buat, V., Le Brun, V., Milliard, B., Kunth, D., Shull, J.M., & Gry, C., 2001, A&A, 375, 805

Dessauges-Zavadsky, M., Calura, F., Prochaska, J.X., D'Odorico, S., & Matteucci, F., 2004, *A&A*, 416, 79

Dickman, R.L., 1978, *ApJS*, 37, 407

Digel, S.W., Lyder, D.A., Philbrick, A.J., Puche, D., & Thaddeus, P., 1996, *ApJ*, 458, 561

Engargiola, G., Plambeck, R.L., Rosolowsky, E., & Blitz, L., 2003, *ApJS*, 149, 343

Fall, S.M., & Pei, Y.C., 1989, *ApJ*, 341, 5

Fernández-Soto, A., Lanzetta, K.M., & Chen, H.W., 2003, *MNRAS*, 342, 1215

Fitzpatrick, E.L., & Massa, D., 1990, *ApJS*, 72, 163

Frerking, M.A., Langer, W.D., & Tielens, A.G.G.M., 1992, *ApJ*, 399, 563

Fukui, Y., Mizuno, N., Yamaguchi, R., Mizuno, A., & Onishi, T., 2001, *PASJ*, 53, 41

Ge, J., & Bechtold, J., 1997, *ApJ*, 477, L73

Ge, J., Bechtold, J., & Black, J.H., 1997, *ApJ*, 474, 67

Ge, J., & Bechtold, J., 1999, in Carilli, C.L., Radford, S.J.E., Menten, K.M., & Langston, G.I., eds, *ASP Conf. Series Vol. 156, Highly redshifted radio lines*, p. 121

Ge, J., Bechtold, J., & Kulkarni, V.P., 2001, *ApJ*, 547, L1

Giallongo, E., Cristiani, S., D'Odorico, S., & Fontana, A., 2002, *ApJ*, 568, 9

Gordon, K.D., Clayton, G.C., Misselt, K.A., Landolt, A.U., & Wolff, M.J., 2003, *ApJ*, 594, 279

Gregg, M.D., Lacy, M., White, R.L., Glikman, E., Helfand, D., Becker, R.H., & Brotherton, M.S., 2002, *ApJ*, 564, 133

Haehnelt, M.G., Steinmetz, M., & Rauch, M., 1998, *ApJ*, 495, 647

Heyer, M.H., Carpenta, J.M., & Snell, R.L., 2001, *ApJ*, 551, 852

Hirashita, H., Ferrara, A., Wada, K., & Richter, P., 2003, *MNRAS*, 341, 18

Hirashita, H., & Ferrara, A., 2005, *MNRAS*, 356, 1529

Hurwitz, M., Jelinsky, P., & Dixon, W.V., 1997, *ApJ*, 481, 31

Johnson, C.T., Burke, P.G., & Kingston, A.E., 1987, *J. Phys. B*, 20, 2553

Jura M., 1974, *ApJ*, 191, 375

Jura M., 1975, *ApJ*, 197, 581

Khare, P., Kulkarni, V.P., Lauroesch, J.T., York, D.G., Crotts, A.P.S., & Nakamura, O., 2004, *ApJ*, 616, 86

Lacy, J., Knacke, R., Geballe, T.R., & Tokunaga, A.T., 1994, *ApJ*, 428, 69

Lanzetta, K.M., Wolfe, A.M., & Turnshek, D.A., 1987, *ApJ*, 322, 739

Launay, J.M., & Roueff, E., 1977, *A&A*, 56, 289

Ledoux, C., Srianand, R., & Petitjean, P., 2002, *A&A*, 392, 781

Ledoux, C., Petitjean, P., & Srianand, R., 2003, *MNRAS*, 346, 209

Leithere, C., Ferguson, H.C., Heckman, T.M., & Lowenthal, J.D., 1995, *ApJ*, 454, 19

Levshakov, S.A., Foltz, C.B., Chaffee F.H., & Black, J.H., 1988, *AJ*, 98, 2052

Levshakov, S.A., Dessauges-Zavadsky, M., D'Odorico, S., & Molaro, P., 2002, *ApJ*, 565, 696

Liszt, H., 2002, *A&A*, 389, 393

Lu, L., Sargent, W.L.W., Barlow, T.A., Churchill, C.W., & Vogt, S., 1996, *ApJS*, 107, 475

Meyer, D.M., York, D.G., Black, J. H., Chaffee, F.H.Jr., & Foltz, C.B., 1986, *ApJ*, 308, L37

Meyer, D.M., & York, D.G., 1992, *ApJ*, 399, 121

Mizuno, N., Yamaguchi, R., Mizuno, A., Rubio, M., Abe, R., Saito, H., Onishi, T., Yonekura, Y., Yamaguchi, N., Ogawa, H., & Fukui, Y., 2001a, *PASJ*, 53, 971

Mizuno, N., Rubio, M., Mizuno, A., Yamaguchi, R., Onishi, T., & Fukui, Y., 2001b, *PASJ*, 53, 45

Molaro, P., Levshakov, S.A., D'Odorico, S., Bonifacio, P., & Centurión, M., 2001, *ApJ*, 549, 90

Malhotra, S., 1997, *ApJ*, 488, 101

Murphy, M.T., & Liske, J., 2004, *MNRAS*, 354, 31

Paglione, T.A.D., Wall, W.F., Young, J.S., Heyer, M.H., Richard, M., Goldstein, M., Kaufman, Z., Nantais, J., & Perry, G., 2001, *ApJS*, 135, 183

Pei, Y.C., 1992, *ApJ*, 395, 130

Pei, Y.C., Fall, S.M., & Bechtold, J., 1991, *ApJ*, 378, 6

Péroux, C., Petitjean, P., Aracil, B., & Srianand, R., 2002, *New Astronomy*, 7, 577

Petitjean, P., Srianand, R. & Ledoux, C., 2000, *A&A*, 364, L26

Petitjean, P., Srianand, R., & Ledoux, C., 2002, *MNRAS*, 332, 383

Pettini, M., Smith, L.J., Hunstead, R.W., & King, D.L., 1994, *ApJ*, 426, 79

Pettini, M., King, D.L., Smith, L.J., & Hunstead, R.W., 1997, *ApJ*, 478, 536

Pettini, M., Ellison, S.L., Steidel, C.C., Shapley, A.E., & Bowen, D.V., 2000, *ApJ*, 532, 65

Prochaska, J.X., & Wolfe, A.M., 1997, *ApJ*, 487, 73

Prochaska, J.X., & Wolfe, A.M., 1999, *ApJS*, 121, 369

Prochaska, J.X., Wolfe, A.M., Tytler, D., Burles, S., Cooke, J., Gawiser, E., Kirkman, D., O'Meara, J.M., & Storrie-Lombardi, L., 2001, *ApJS*, 137, 21

Prochaska, J.X. & Wolfe, A.M., 2002, *ApJ*, 566, 68

Reimers, D., Baade, R., Quast, R., & Levshakov, S.A., 2003, *A&A*, 410, 785

Richards, G.T., & SDSS collaborators, 2002, *AJ*, 123, 2945

Roueff, E., & Le Bourlet, J., 1990, *A&A*, 236, 515

Sargent, W.L.W., Steidel, C.C., & Boksenberg, A., 1988, *ApJS*, 68, 539

Schirber, M., & Bullock, J.S., 2003, *ApJ*, 584, 110

Schröder, K., Staemmler, V., Smith, M. D., Flower, D. R., & Jaquet, R., 1991, *J. Phys. B*, 24, 2487

Scott, J., Bechtold, J., Morita, M., Dobrzychki, A., & Kulkarni, V.P., 2002, *ApJ*, 571, 665

Shull, J.M., Tumlinson, J., Jenkins, E.B., Moos, H.W., Rachford, B.L., Savage, B.D., Sembach, K.R., Snow, T.P., Sonneborn, G., York, D.G., Blair W.P., Green, J.C., Friedman, S.D., & Sahnow, D.J., 2000, *ApJ*, 538, L73

Solomon, P.M., Rivolo, A.R., Barrett, J., & Yahil, A., 1987, ApJ, 319, 730

Songaila, A., Cowie, L.L., Vogt, S., Keane, M., Wolfe, A.M., Hu, E.M., Oren, A.L., Tytler, D.R., & Lanzetta, K.M., 1994, Nature, 371, 43

Spitzer, L., & Cochran, W.D., 1973, ApJ, 186, 23

Spitzer, L., & Zweibel, E.G., 1974, ApJ, 191, 127

Spitzer, L., Cochran, W.D., & Hirshfeld, A., 1974, ApJS, 28, 373

Srianand, R., Petitjean, P., & Ledoux, C., 2000, Nature, 408, 931

Srianand, R., & Petitjean, P., 2001, A&A, 373, 816

Steidel, C.C., & Sargent, W.L.W., 1992, ApJS, 80, 1

Staemmler, V., & Flower, D. R., 1991, J. Phys. B, 24, 2343

Storrie-Lombardi, L.J., & Wolfe, A.M., 2000, ApJ, 543, 552

Strong, A.W., Bloemen, J.B.G.M., Dame, T.M., Grenier, I.A., Hermsen, W., Lebrun, F., Nyman, L.A., Pollock, A.M.T., & Thaddeus, P., 1988, A&A, 207, 1

Takahashi, J., & Uehara, H., 2001, ApJ, 561, 843

Tielens, A.G.G.M., & Hollenbach, D.J., 1985, ApJ, 291, 722

Vanden Berk, & SDSS collaborators, 2001, AJ, 122, 549

Vladilo, G., 1998, ApJ, 493, 583

Vreeswijk, P.M., Ellison, S.L., Ledoux, C., Wijers, R.A.M.J., Fynbo, J.P.U. *et al.*, 2004, A&A, 419, 927

Williams, J.P., & McKee, C.F., 1997, ApJ, 476, 166

Wolfe, A.M., & Davis, M.M., 1979, AJ, 84, 699

Wolfe, A.M., Prochaska, J.X., & Gawiser, E., 2003a, ApJ, 593, 215

Wolfe, A.M., Gawiser, E., & Prochaska, J.X., 2003b, ApJ, 593, 235

Wolfe, A.M., Howk, J.C., Gawiser, E., Prochaska, J.X., & Lopez, S., 2004, ApJ, 615, 625

Wolfire, M.G., Hollenbach, D., McKee, C.F., Tielens, A.G.G.M., & Bakes, E.L.O., 1995,
ApJ, 443, 152

Wolniewicz, L., Simbotin, I., & Dalgarno, A., 1998, ApJS, 115, 293

Table 3. H_2 column densities^a, b -parameter and redshift

Parameter	Measured value	1σ error
z	1.776553	0.000003
b (km s ⁻¹)	13.85	0.52
$\log(N_{J=0})$	19.144	0.066
$\log(N_{J=1})$	19.467	0.043
$\log(N_{J=2})$	17.901	0.187
$\log(N_{J=3})$	17.674	0.184
$\log(N_{J=4})$	15.101	0.125
$\log(N_{\text{total}})$	19.648	0.035

^aColumn densities are in units of cm⁻².

Table 4: H_2 absorption in redshifted DLA and sub-DLA systems

Object	z_{abs}	$\log N(\text{HI})$	$\log f_{\text{H}_2}$	$[\frac{\text{Zn}}{\text{H}}]^a$	$[\frac{\text{Fe}}{\text{H}}]^b$	$\frac{E_{\text{B-V}}}{0.01}^c$	Ref
Q0000 – 263	3.390	21.41 ± 0.08	< -6.98	-2.07 ± 0.10	-2.04 ± 0.09	0.00 ± 0.33	2
Q0010 – 002	2.025	20.80 ± 0.10	< -6.09	-1.20 ± 0.12	-1.25 ± 0.11	0.20 ± 0.67	1
Q0013 – 004	1.973	20.83 ± 0.04	-2.81 ± 0.64	-0.75 ± 0.06	-1.51 ± 0.05	4.65 ± 0.90	3
Q0013 – 004	1.968	≤ 19.43	≥ -2.36	≥ -0.73	≥ -2.33		3
Q0058 – 292	2.671	21.00 ± 0.10	< -6.69	-1.42 ± 0.11	-1.76 ± 0.10	0.97 ± 0.54	1
Q0100 + 130	2.309	21.40 ± 0.05	< -5.30	-1.62 ± 0.06	-1.93 ± 0.05	1.44 ± 0.45	5,6
Q0102 – 190	2.370	20.85 ± 0.08	< -5.60	-1.73 ± 0.14	-1.89 ± 0.13	0.19 ± 0.24	1
Q0112 – 306	2.418	20.37 ± 0.08	< -5.72		-2.50 ± 0.09		1
Q0112 – 306	2.702	20.15 ± 0.07	< -5.50		-0.89 ± 0.10		1
Q0112 + 029	2.423	20.70 ± 0.10	< -6.32	$-1.14 \pm 0.13^*$	-1.35 ± 0.11	0.47 ± 0.43	1
Q0135 – 273	2.800	20.80 ± 0.10	< -6.40	$-1.29 \pm 0.17^*$	-1.54 ± 0.15	0.48 ± 0.49	1
Q0347 – 383	3.025	20.56 ± 0.05	-5.71 ± 0.10	-0.98 ± 0.09	-1.72 ± 0.06	1.46 ± 0.41	1
Q0405 – 443	2.550	21.00 ± 0.15	< -6.59	-1.17 ± 0.16	-1.52 ± 0.15	1.75 ± 1.40	1
Q0405 – 443	2.595	20.90 ± 0.10	-2.44 ± 0.23	-1.02 ± 0.12	-1.33 ± 0.11	1.81 ± 1.15	1
Q0405 – 443	2.621	20.25 ± 0.10	< -6.15		-2.15 ± 0.10		1
Q0454 + 039	0.860	20.69 ± 0.06	< -4.10	-1.03 ± 0.12	-1.02 ± 0.08	0.00 ± 0.72	6,7
Q0458 – 020	2.040	21.65 ± 0.09	< -5.70	-1.19 ± 0.09	-1.77 ± 0.10	9.95 ± 3.57	5,6
Q0515 – 441	1.151	19.88 ± 0.05	-2.64 ± 0.30	-0.54 ± 0.05	$-1.55 \pm 0.10^{**}$	0.96 ± 0.28	8
Q0528 – 250	2.811	21.20 ± 0.10	-2.58 ± 0.22	-0.78 ± 0.12	-1.25 ± 0.15	8.14 ± 4.14	1,9,1
Q0551 – 366	1.962	20.50 ± 0.08	-2.78 ± 0.90	-0.15 ± 0.09	-0.95 ± 0.09	8.82 ± 2.73	4
Q0841 + 129	2.374	20.90 ± 0.10	< -5.93	-1.52 ± 0.14	-1.71 ± 0.11	0.40 ± 0.42	1,5,1
Q0841 + 129	2.476	20.65 ± 0.10	< -6.05	-1.52 ± 0.11	-1.51 ± 0.11	0.00 ± 0.23	1,5,1
Q0935 + 417	1.373	20.40 ± 0.10	< -3.70	-0.80 ± 0.14	$-0.90 \pm 0.20^{**}$	0.40 ± 1.92	6,11
Q1037 – 270	2.139	19.70 ± 0.10	< -5.40	-0.26 ± 0.11	-0.65 ± 0.10	0.76 ± 0.39	12
Q1101 – 264	1.839	19.35 ± 0.04	< -4.75	$-0.82 \pm 0.14^*$	-1.36 ± 0.05	0.08 ± 0.04	1
Q1117 – 133	3.351	20.85 ± 0.10	< -6.37	-1.28 ± 0.13	-1.55 ± 0.13	0.81 ± 0.62	1,13
Q1157 + 014	1.944	21.70 ± 0.10	< -6.69	-1.32 ± 0.10	-1.73 ± 0.10	6.86 ± 3.19	1
Q1223 + 178	2.466	21.40 ± 0.10	< -6.80	-1.63 ± 0.11	-1.70 ± 0.10	0.41 ± 0.89	1,5
Q1232 + 082	2.338	20.90 ± 0.10	≥ -3.41		-1.73 ± 0.13		10,1
Q1328 + 307	0.692	21.28	< -5.30	-1.21	-1.66	3.55	6,15
Q1331 + 170	1.776	21.18 ± 0.04	-1.25 ± 0.05	-1.22 ± 0.04	-2.09 ± 0.04	3.69 ± 0.52	16
Q1337 + 113	2.508	19.95 ± 0.05	< -5.37		-2.05 ± 0.07		1
Q1337 + 113	2.796	20.85 ± 0.08	< -6.54		-2.02 ± 0.09		1
Q1444 + 014	2.087	20.07 ± 0.07	-1.48 ± 0.38	-0.60 ± 0.15	-1.58 ± 0.09	1.24 ± 0.52	1
Q1451 + 123	2.469	20.30 ± 0.10	< -4.70		-2.41 ± 0.10		1
Q1451 + 123	3.171	19.90 ± 0.20	< -5.80		-2.09 ± 0.24		1
Q1946 + 766	2.843	20.27 ± 0.06	< -5.05		-2.53 ± 0.06		5,6
Q2059 – 360	2.508	20.14 ± 0.07	< -4.93	$-1.76 \pm 0.09^*$	-2.12 ± 0.05	0.02 ± 0.17	1
Q2059 – 360	3.083	20.85 ± 0.08	< -6.64	$-1.65 \pm 0.12^*$	-1.83 ± 0.18	0.17 ± 0.17	1
Q2138 – 444	2.852	20.82 ± 0.05	< -6.87	-1.48 ± 0.05	-1.68 ± 0.05	0.38 ± 0.15	1